# 國 立 交 通 大 學

# 電信工程學系

# 碩 士 論 文

IEEE 802.15.3c 無線個人區域網路之單載波
區塊傳輸基頻接收機的設計與模擬

Design and Simulation of the Baseband Receiver for Single

Carrier Block Transmission in IEEE 802.15.3c

Wireless Personal Area Network

研究生：汪奕廷

指導教授：黃家齊 博士

中 華 民 國 九 十 八 年 六 月

# IEEE 802.15.3c 無線個人區域網路之單載波區塊傳輸基頻接收機的設計與模擬

Design and Simulation of the Baseband Receiver for Single Carrier Block Transmission in IEEE 802.15.3c Wireless Personal Area Network

研 究 生：汪奕廷　　　　　　Student：Yi-Ting Wang

指導教授：黃家齊 博士　　　　Advisor：Dr. Chia-Chi Huang

國 立 交 通 大 學

電信工程學系

碩 士 論 文

A Thesis

Submitted to Department of Communication Engineering

College of Electrical and Computer Engineering

National Chiao Tung University

in partial Fulfillment of the Requirements

for the Degree of

Master of Science

in

Communication Engineering

June 2009

Hsinchu, Taiwan, Republic of China

中華民國九十八年六月

# IEEE 802.15.3c 無線個人區域網路之單載波區塊傳輸基頻接收機的設計與模擬

學生：汪奕廷　　　　　　　　　　　　　指導教授：黃家齊博士

國立交通大學電信工程學系 碩士班

## 摘　　要

　　為了提供室內高速個人區域網路的需求，IEEE 802.15.3c 的標準被制定出來。它兼採單載波區塊傳輸和正交頻分多工兩種調變方式，操作在 60GHz 免認證頻段，所提供的傳輸速率為 1 Gbps 以上。這篇論文將依據 IEEE 802.15.3c 標準內單載波區塊傳輸所規定的封包格式設計其基頻接收機架構，其中包含符元時序估計、通道估計、頻域等化器、及資料檢測等部分。每個部分將針對其運作原理及演算法做詳細的介紹，在每個部分中盡可能在性能表現與運算複雜度間取一平衡點。為了驗證接收機的效能，我們進行各種電腦模擬，特別在資料檢測的部分我們會提出各種方法來提升接收機在位元錯誤率上的表現，並計算其運算複雜度作為參考。最後我們提出結論與未來的研究方向。

Design and Simulation of the Baseband Receiver for Single Carrier Block
Transmission in IEEE 802.15.3c Wireless Personal Area Network

Student：Yi-Ting Wang                    Advisors：Dr. Chia-Chi Huang

Department of Communication Engineering
National Chiao Tung University

## ABSTRACT

The IEEE 802.15.3c WPAN standard was defined in order to support the demand of high data rate indoor transmission. It adopts SCBT and OFDM modulations and operates at 60 GHz unlicensed band. Hope to provide data rates more than 1 Gbps. In this thesis, we propose an IEEE 802.15.3c SCBT baseband receiver architecture according to its specified frame format. The receiver includes symbol timing estimation, channel estimation, frequency domain equalization, and data detection. We will describe the operation principles and the algorithms of each block in details. And we try to make a tradeoff between system performance and computation complexity. In order to verify the performance of the receiver, computer simulations are conducted under different conditions. Especially in data detection part, we propose several methods to enhance the performance of the receiver in BER, and we will calculate the complexity of computation as references as well. Finally, we draw conclusions and comments on possible future research directions.

# 誌　　　謝

首先要感謝我的指導老師黃家齊教授在這兩年來的指導，提供了良好的學習與研究環境使我得以專注在學業上並順利完成這兩年的學業。另外特別感謝古孟霖學長總是不厭其煩的與我討論我的研究，並提供了許多經驗幫我解決了許多問題，使我收穫良多。並感謝口試招集人吳文榕教授、委員陳紹基教授與高銘盛教授，提供許多寶貴的意見使得我的論文能更為完整。

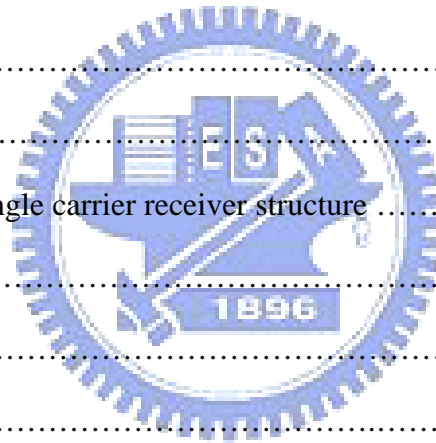接著感謝我親愛的家人們從小到大對我的栽培與照顧，在外念書的期間雖然總是聚少離多，但他們依舊願意給我溫暖與後盾在背後支持著、鼓勵著我，讓我能夠心無旁騖的完成自身的學業。

感謝同為碩二的同學們冠群、丁丁、王森和小顗這兩年來的照顧與陪伴，彼此之間的幫忙扶持讓上課與研究都更加的有趣與踏實。另外也感謝碩班的學長姐，阿威、建勳、文娟與思潔還有學弟妹小馬、煒翰、詠仁與佳儀，雖然相處的時間不多，但這一切都因為有你們而更加的充實。

另外感謝 NTL 實驗室的朋友們，雖然是在偶然的情況下認識，但你們總是願意把我當成實驗室的一分子關心著我，讓我倍感溫暖。還要感謝一起打球的朋友們，歪歪、黑人、Sony、忠傑、Sky 等人，還有從大學起就一路照顧著我的紹峰學長，與你們打球的時間和比賽的過程都是我相當珍貴的回憶。

最後我要感謝我的女朋友簡家齊，在交往的過程中總是體貼著我，給我很多精神上的支持與鼓勵，讓我更有勇氣並且積極的面對一切的困難與挑戰。

# Contents

# List of Tables

# List of Figures

vii

## Chapter 1 Introduction

To respond the demands for very high data rates indoor wireless communication such as uncompressed high definition video streaming, flash file downloading and so on, many applications for high speed and short range transmission are being standardized. For example, IEEE 802.11 very high throughput (VHT) and wireless HD are proposed. IEEE 802.15.3c wireless personal area network (WPAN) is one of them to satisfy such requirements. In this chapter, we will briefly describe the situation of this standard including potential, requirements, and challenges. And we will introduce organization of this thesis at the end of this chapter as well.

## 1.1 IEEE 802.15.3c WPAN
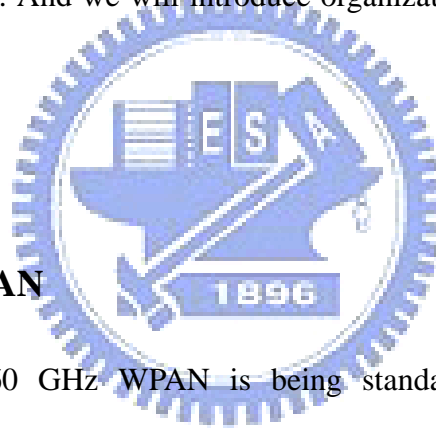
The millimeter-wave 60 GHz WPAN is being standardized by the IEEE 802.15 Alternative PHY Task Group 3c (IEEE 802.15.3c). This emerging IEEE 802.15.3c standard targets the data rates of multi-giga bits per second (multi-Gbps) for short range around 5 to 10 meters indoor applications [1].

The realization of such high speed wireless transmission has long been obstructed mainly by two critical factors: one is the lack of spectrum which is wide enough and the other is the high cost of high frequency circuits and device. Recently, the substantial unlicensed spectrum became available at the millimeter-wave band of 60 GHz. Also, the advancement in

technology drives the cost of 60 GHz circuits and devices much lower than in the past.

There are two kinds of systems in this standard. One is the OFDM mode, and the other is the single carrier (SC) mode. Common mode which enables the IEEE 802.15.3c devices having different PHYs (SC and OFDM) to communicate with each other, and it is therefore a key technique for standardization to realize flexible systems with easy expandability from SC to OFDM or other SCs and vice versa. After comparing SC with OFDM, we found that SC system is more suitable in application in IEEE 802.15.3c WPAN system. We focus on SC system receiver design only in this paper.

## 1.2 Challenges

Despite its huge potentials to achieve Gbps data rate, 60 GHz system has a number of technical challenges and many open issues to be solved before its full deployment. One of them is channel propagation issue, which causes significantly higher path loss at 60 GHz than those at lower frequencies. According to this issue, the propagation range of 60 GHz must be shorter, usually in 5 to 10 meters, than other system. Although the price of such high speed circuit is much lower than in the past, the peak to average power ratio (PAPR) issue still remains in transceiver design. Another important issue is the computation complexity of the system. To achieve such high data rates, the design of the system structures and the methods for SCBT baseband receiver can't be too complicated.

## 1.3 About the thesis

This paper is organized as following. Chapter 2 compares the SC and OFDM systems. Then we will introduce the advantages and remaining issues of each system. In chapter 3, we will give a simple introduction of IEEE 802.15.3c standard draft 3. We focus on the PHY layer specification, and base on this standard to develop our baseband receiver. The baseband receiver that we proposed will be shown in chapter 4. The receiver contains synchronization, channel estimation, equalization, and data detection parts. The simulation results of each part in SC receiver will be shown in chapter 5. Finally, we will make our conclusions and future works in the last chapter, chapter 6.

## Chapter 2 Single carrier (SC) system (vs. OFDM)

In this chapter, we will introduce the SC system. And we will make a comparison between SC and OFDM systems. Some open issues of OFDM system such as PAPR issue, effect of carrier frequency offset (CFO), and so on will be mentioned at later of this chapter. According to the requirements of our system, SC system outperforms OFDM system. So we choose the SC system as our proposed receiver structure for IEEE 802.15.3c WPAN. At last, we will simply introduce the single carrier block transmission (SCBT) system in the end of this chapter.

## 2.1 Compare with OFDM

Orthogonal frequency division multiplexing (OFDM) has already been included in digital audio/video broadcasting (DAB/DVB) standard in Europe, and has been successfully applied to high-speed digital subscriber line (DSL) modems in the United States.

To annihilate inter-block interference (IBI) between successive inverse fast Fourier transform (IFFT) processed blocks, a cyclic prefix (CP) of length no less than the channel order is inserted per transmitted block. Discard the CP at the receiver not only suppresser IBI, but also converts the linear channel convolution into circular convolution, which means after converted by FFT the channel frequency will be one tap for each sub-carrier. By implementing IFFT at the transmitter and FFT at the receiver, OFDM converts an

inter-symbol interference (ISI) channel into parallel ISI-free sub-channels with gains equal to channel frequency response values on FFT grid.

Although OFDM enables simple equalization, it introduces the following three well-known problems: one is the PAPR of the transmitted signal power is large, necessitating power back off. SC modulation uses a single carrier, instead of the many typically used in OFDM, so the PAPR is smaller than multi-carrier systems. The other is that OFDM system is very sensitive to transmit-receive oscillator mismatch which cause CFO. The last problem is that the uncoded OFDM system does not enable the available multipath diversity, as described in [2].

Consortium of Millimeter wave Practical Applications (CoMPA) has been established to promote single carrier (SC) modulation for the future WPAN system. This is because SC modulation has several advantages in realizing low-cost and low-power consumption devices over multi-carrier modulation especially in short range communications environment [3].
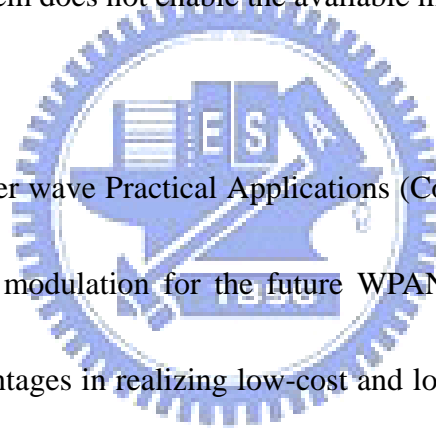
## 2.2 Single Carrier Block Transmission (SCBT)

In order to reduce the complexity of equalization, we copy the last part of each single carrier data block as CP which is the same operation as OFDM time domain signals. Then we can equalize the ISI caused by multi-path effect by one-tap equalizer on each subcarrier in frequency domain. This system is called single carrier block transmission (SCBT) system.

Moreover, from figure 2.1 and figure 2.2, we can easily found that the difference between

SCBT and OFDM systems is only the position of IFFT operation, but the overall system

complexities remain the same.

OFDM Tx

Encoding — S/P — IFFT — P/S — Add CP

SCBT Tx

Encoding ——————————————— Add CP
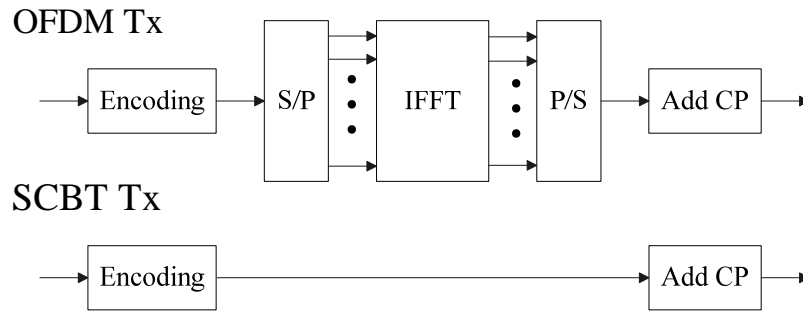
Figure 2.1 OFDM and SCBT Tx

OFDM Rx

Remove CP — S/P — FFT — Frequency domain Equalization — P/S — Decoding

SCBT Rx

Remove CP — S/P — FFT — Frequency domain Equalization — IFFT — P/S — Decoding
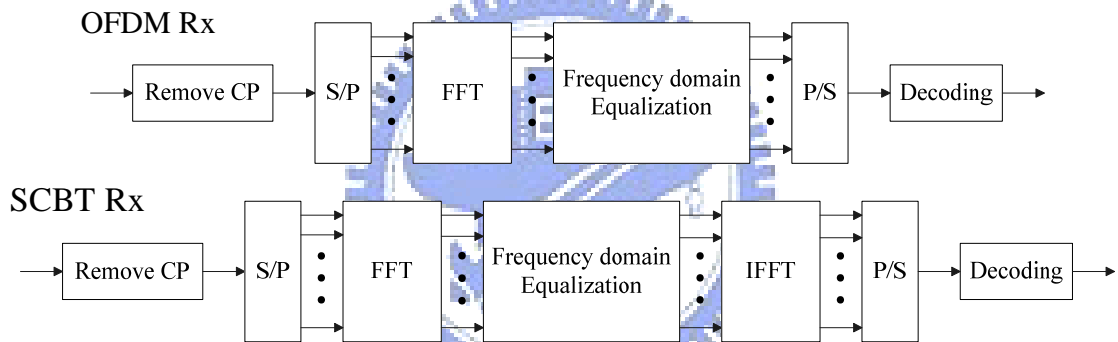
Figure 2.2 OFDM and SCBT Rx

Compare to OFDM system, SCBT system with frequency domain equalization has

similar performance, efficiency, and low signal processing complexity advantages as OFDM.

SCBT system also has several advantages. SCBT system reduces PAPR requirement. This in

turn means that the power amplifier of the SC transmitter requires a smaller linear range to

support the given average power. This enables the use of a cheaper power amplifier than a

comparable OFDM system, as mentioned in [4]. And in addition are less sensitive than

OFDM to radio frequency (RF) impairments such as CFO which caused by the mismatch of

6

oscillators in transmitter and receiver. According to these attractive features, we choose the

SCBT system as our 60 GHz receiver.

In figure 2.3 and 2.4, we can easily find the performances for SCBT system are much

better than OFDM system in BER comparison. Furthermore, the BER curves for OFDM are

almost the same. That because the signals in OFDM are carried by frequency, and it can't

obtain any diversity from multipath fading channel. The performances for SCBT are quite

different according to the different path numbers. More path number gets better performance.

Different from OFDM system, the signals in SCBT system can gain diversity in time domain

from multipath fading channel.
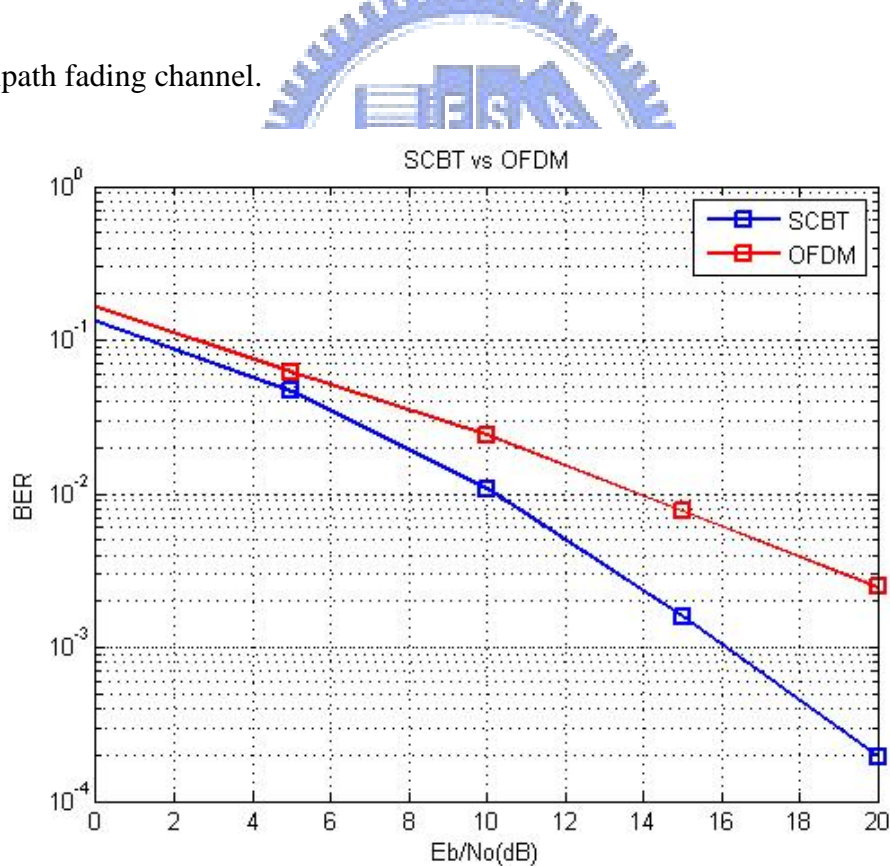


Figure 2.3 Performances for SCBT and OFDM system in 2-path channel
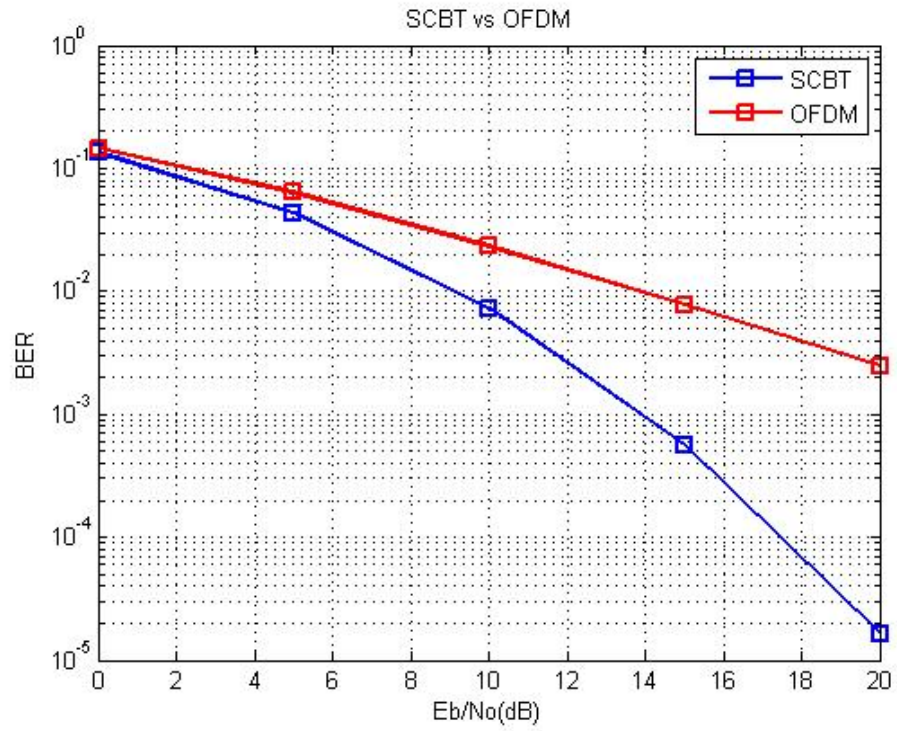
Figure 2.4 Performances for SCBT and OFDM system in 6-path channel
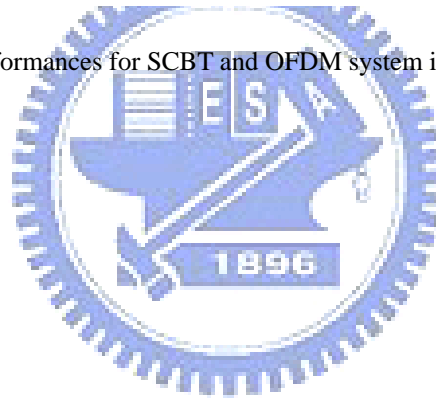
# Chapter 3 IEEE 802.15.3c WPAN PHY standard

In this chapter, we will introduce IEEE 802.15.3c physical layer specification. Include channelization in 60 GHz unlicensed band, frame format which contains the structure of headers, preambles, and data symbols, and the physical (PHY) layer convergence protocol (PLCP) preamble which contains the information for synchronization (SYNC) and channel estimation (CE).

## 3.1 Channelization

IEEE 802.15.3c WPAN is operated at 60GHz unlicensed band. Divide this frequency band into four independent channels. Figure 3.1 and 3.2 show the channel plans of full and half rate transmission. The detail parameters of these four channels are listed in table 3.1 and 3.2 which are full rate and half rate, respectively.
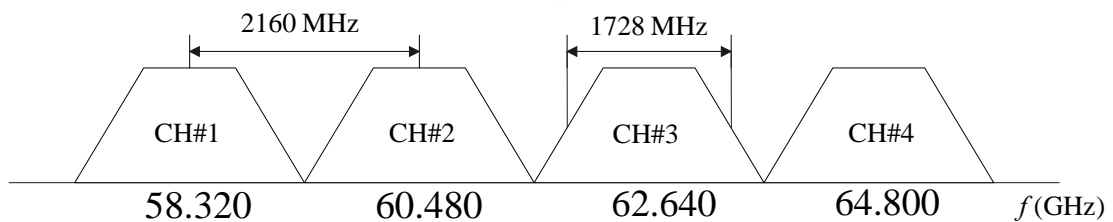


Figure 3.1 IEEE 802.15.3c channel plan (full rate)
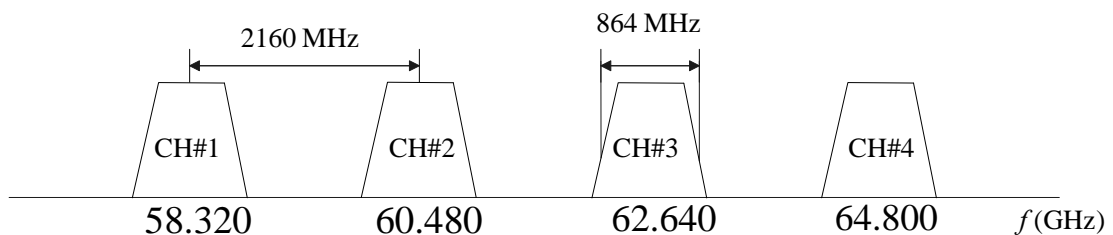


Figure 3.2 IEEE 802.15.3c channel plan (half rate)

| Channel number | Low freq. (GHz) | Center freq. (GHz) | High freq. (GHz) | Nyquist BW (MHz) | Roll off factor |
|---|---|---|---|---|---|
| CH#1 | 57.240 | 58.320 | 59.400 | 1728 | 0.25 |
| CH#2 | 59.400 | 60.480 | 61.560 | 1728 | 0.25 |
| CH#3 | 61.560 | 62.640 | 63.720 | 1728 | 0.25 |
| CH#4 | 63.720 | 64.800 | 65.880 | 1728 | 0.25 |

Table 3.1 Parameters of IEEE 802.15.3c channel plan (full rate)

| Channel number | Low freq. (GHz) | Center freq. (GHz) | High freq. (GHz) | Nyquist BW (MHz) | Roll off factor |
|---|---|---|---|---|---|
| CH#1 | 57.240 | 58.320 | 59.400 | 1728 | 0.25 |
| CH#2 | 59.400 | 60.480 | 61.560 | 1728 | 0.25 |
| CH#3 | 61.560 | 62.640 | 63.720 | 1728 | 0.25 |
| CH#4 | 63.720 | 64.800 | 65.880 | 1728 | 0.25 |

Table 3.2 Parameters of IEEE 802.15.3c channel plan (half rate)

## 3.2 Frame Format

Frame format that includes a preamble providing sufficient robustness against wireless environment being subject to the characteristics of millimeter wave. Each of the sequences in

10

the preamble is Golay code, which realizes a reduced SYNC circuit, and which can also be

shared with the channel estimator.

Figure 3.3 shows the proposed frame format for IEEE 802.15.3c standardization. The

frame format consists of a PHY preamble, frame header, and frame payload including pilot

channel estimation sequence (PCES) and data slot. Frame header contains PHY and MAC

headers which include the information that used in PHY and MAC layers. The PHY preamble

which is also named PLCP preamble will be introduced in detail in next section.

| PHY Preamble (long, short, or middle) | Frame Header | Frame Payload |
|---|---|---|
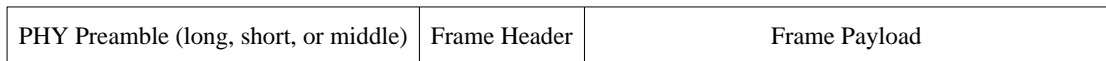
Figure 3.3 IEEE 802.15.3c Frame Format

The structure of frame payload is shown in figure 3.4. A data slot consists of cyclic

prefix pilot symbols (CPPS) with different length and SCBT data blocks with two sizes, 256

and 512. The most important role of CPPS is used as CP for frequency domain equalization

which is used for compensating the multi-path effect. The PCES here is used for timing

tracking, CFO compensation, and more accurate channel estimation. More parameters of

IEEE 802.15.3c frame format are listed in table 3.3.

| $a_M$ | SCBT data block | $a_M$ | SCBT data block | • • • | $a_M$ | SCBT data block | $a_M$ |
|---|---|---|---|---|---|---|---|

| PCES | Data Slot | PCES | Data Slot | • • • | PCES | Data Slot |
|---|---|---|---|---|---|---|

| Frame Payload |
|---|
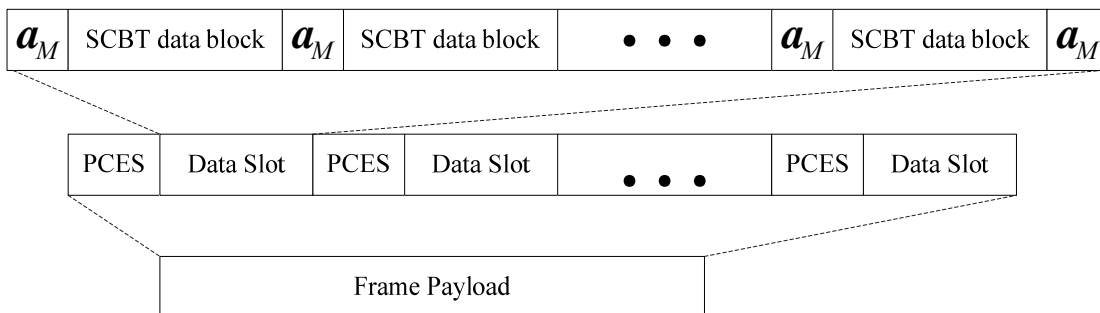
Figure 3.4 Structure of Frame Payload

| Data block size | PCES length | PCES period | CPPS length |
|---|---|---|---|
| 256 (mandatory) | 768 | 8192, 16384, or 32768 | 16, 32, or 64 |
| 512 (option) | 1536 | 8192, 16384, or 32768 | 32, 64, 96, or 128 |

Table 3.3 IEEE 802.15.3c frame format parameters

## 3.3  PLCP Preamble

Figure 3.5 illustrates the structure of PHY preamble defined in IEEE 802.15.3c SCBT system. The preamble consists of synchronization sequence, start frame delimiter (SFD), and channel estimation sequence. There are the long, medium, and short preambles can be chosen to deal with different requirements or transmission modes. The preambles can be selected according to the information contained in the PHY header. Synchronization sequence is constructed by 32, 16, or 8 Golay code with 128 chips. According to the correlation property of Golay code with 128 chips, we can develop our symbol timing tracking algorithm by using matched filter. SFD is also constructed by Golay code with 128 chips. Base on the special arrangement of these 4 Golay codes with 128 chips, we can estimate when the synchronization sequence is over and get the starting timing in channel estimation part and data detection part. Channel estimation sequence consists of two complementary sequences of length 256 with both cyclic prefix and postfix. We develop our channel estimation algorithm by using the special auto-correlation property of complementary sequences.

Figure 3.5 IEEE 802.15.3c PHY preamble structure

## Chapter 4 IEEE 802.15.3c single carrier receiver structure

From previous chapters, we know synchronization, channel estimation, equalization, and data detection are very important in IEEE 802.15.3c SC receiver design. Synchronization means symbol timing estimation. In SCBT system, we need to know the timing of data block coming. By using the estimated channel state information (CSI) which provided by channel estimator, equalizer can equalize the multi-path channel effect. At last, we use some data detection method to enhance the performance in bit error rate (BER). We will introduce the receiver structure that we design in detail in this chapter.

## 4.1 Block diagram
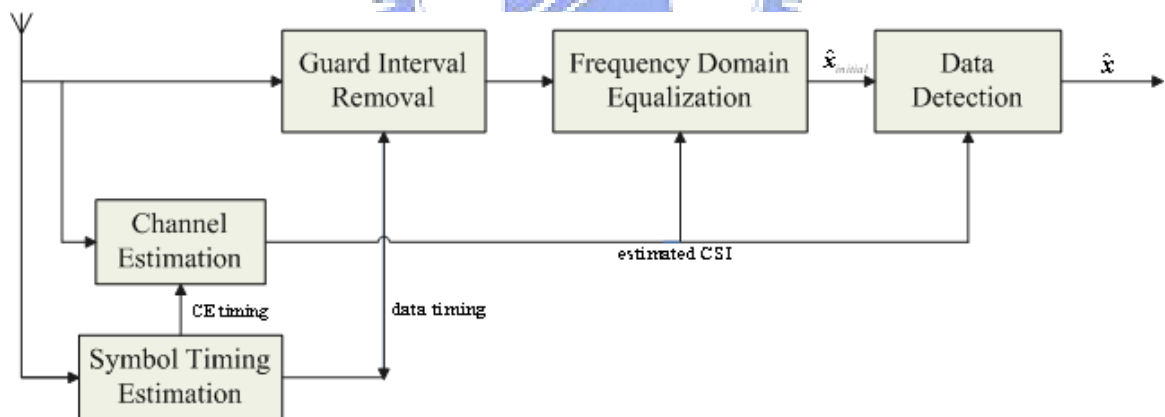


Figure 4.1 SCBT baseband receiver structure

Figure 4.1 shows the proposed SCBT receiver block diagram for IEEE 802.15.3c baseband transmission. The receiver consists of symbol timing estimation, channel estimation, guard interval removal, frequency domain equalization, and data detection.

We assume the CFO is already perfectly compensated before converting the signal to the

baseband. Symbol timing estimation provides the channel estimation timing and the data

sequence timing for follow up applications. In symbol timing estimation, we use the

synchronization sequence in PLCP preamble to get the correct timing for channel estimation

and data detection.

According to the timing provided by the symbol timing estimator, channel estimator

knows when the channel estimation sequence comes and starts to estimate the time domain

impulse responses of the frequency selective fading channel. Then channel estimator passes

these channel state information, including channel impulse responses (CIRs) and noise power,

to the equalizer and data detector.

Before we send the signal into equalizer, we need to remove the CP of data sequence. On

the receiver side of SCBT system, ISI caused by multi-path fading channel is removed by

frequency domain equalization (FDE). FDE can take the form of either zero forcing (ZF) or

minimum mean square error (MMSE). While MMSE-FDE has much better performance than

ZF-FDE, it needs to know signal-to-noise ratio (SNR) at receiver side. We use the FFT

structure here of FDE to simplify the complexity of receiver and get an initial value for data

detection after equalization.

In data detection part, we propose two detection methods to enhance the performance of

FDE. One is the Gibbs Sampler, and another is multi-path interference cancellation (MPIC)

method. These two methods will increase complexity of system lightly. User can decide

whether or not to use these methods which can be replaced by a simple hard decision device.

The algorithms we use in symbol timing estimation, channel estimation, equalization, and

data detection parts will be introduced in detail in following sections.

## 4.2 Synchronization

In IEEE 802.15.3c standard, the synchronization sequence consists of 40, 20, or 12

repetition Golay sequences ($s_{128}$) corresponding to long, medium, or short preamble. The

Golay sequence $s_{128}$ can be represented as hexadecimal form shown in equation 4.1.

$$s_{128} = [05C99C5005369CAFFA3663AF05369CAF].\qquad(4.1).$$

Figure 4.2 shows the structure of synchronization sequence. The former part of

synchronization sequence is used for timing tracking, and the latter part of it is start frame

delimiter which is used for detecting when the synchronization sequence ends.

| $s_{128}$ | $s_{128}$ | • • • | $s_{128}$ | $s_{128}$ | $-s_{128}$ | $s_{128}$ | $-s_{128}$ |
|---|---|---|---|---|---|---|---|

$$\overleftrightarrow{SYNC\ seq.} \qquad \overrightarrow{SFD}$$
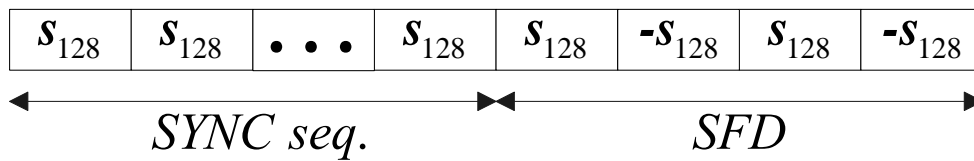
Figure 4.2 IEEE 802.15.3c SCBT synchronization sequence

To develop our synchronization scheme, we need to know the auto-correlation of 128

chips Golay code, $s_{128}$. We define auto-correlation by following equation:

$$R_s[k] = \sum_{n=0}^{127} s[n]s[((n-k))_{128}]\qquad(4.2)$$

for $0 \le k \le 127$ where $((\cdot))_N$ denotes the modulo $N$ operation. Figure 4.3 shows the result of

auto-correlation of $s_{128}$. We observe that peak value occurs when the sequence is totally matched. And the correlation value when is not matched is relatively small comparing with the peak value. By using this special property, we can develop our symbol timing synchronization scheme.
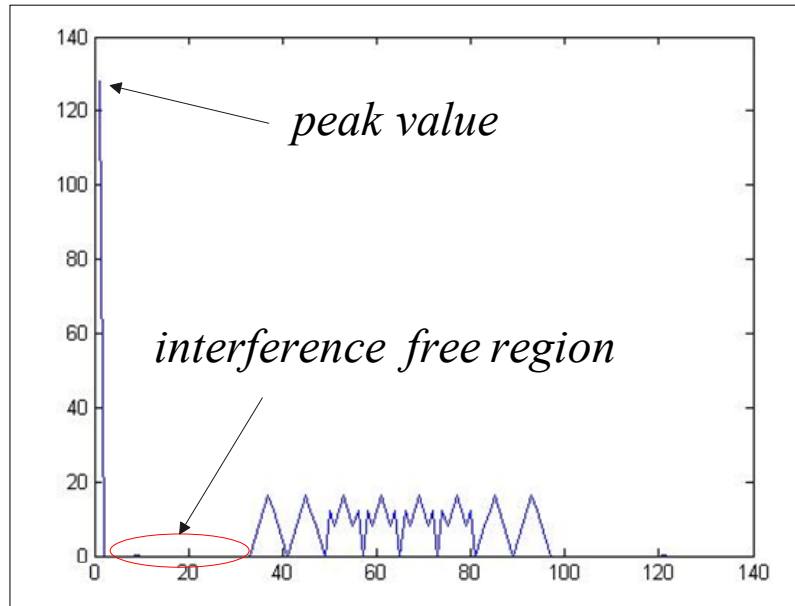


Figure 4.3 Auto-correlation of Golay code with 128 chips
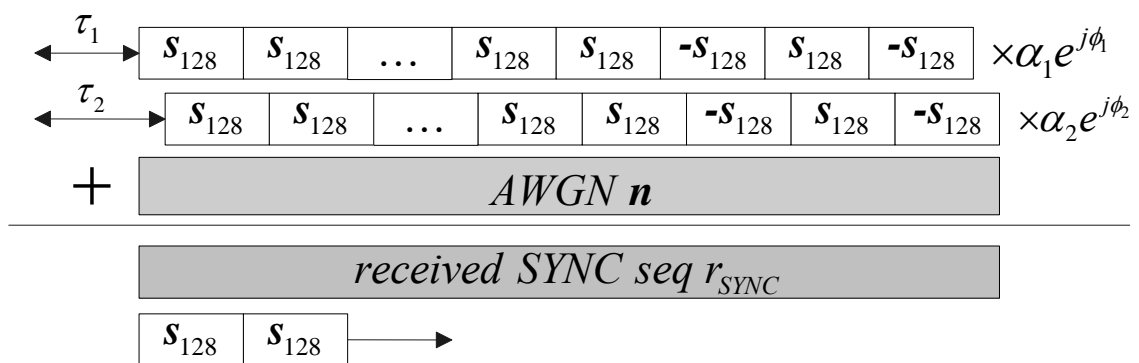


Figure 4.4 An example of received SYNC sequence in two-path channel

A simple case is shown in the above figure. The synchronization sequence passes through a two-path Rayleigh fading channel. Figure 4.4 also shows the relationship between

17

the synchronization sequence and the received signal. To simplify the main topic, we ignore the noise effect in the following deriving. We define the correlation filter window as $s_{sync} = [s_{128}\ s_{128}]$. Then we use the sliding window to calculate the cross-correlation of $r_{sync}$ and $s_{sync}$. We can expect that the peak value will occur when $s_{sync}$ is perfectly matched to the synchronization sequence in the $r_{sync}$. It means the peak value will occur at $\tau_1$, $\tau_2$, $\tau_1 + 128$, $\tau_2 + 128$, $\cdots$, until the SFD appears.

Figure 4.5 is the channel impulse response, and figure 4.6a is the output sequence of correlation detector. We can easily find that peak values occur repeatedly. We overlap the channel impulse responses with processing gain 256 on the output sequence in figure 4.6b, and find they are almost the same. When the SFD passes through the filter, the peak value will occur with 180 degrees phase rotation. According to these peak values and the phase rotation, we can easily find the position of the strongest path and the timings when channel estimation sequence and data sequence come.
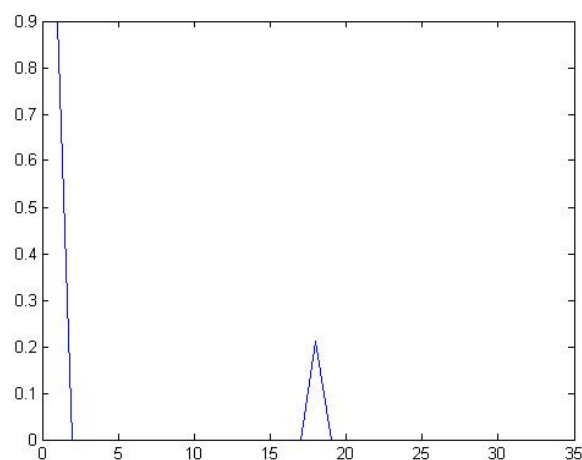


Figure 4.5 Two-path channel impulse responses
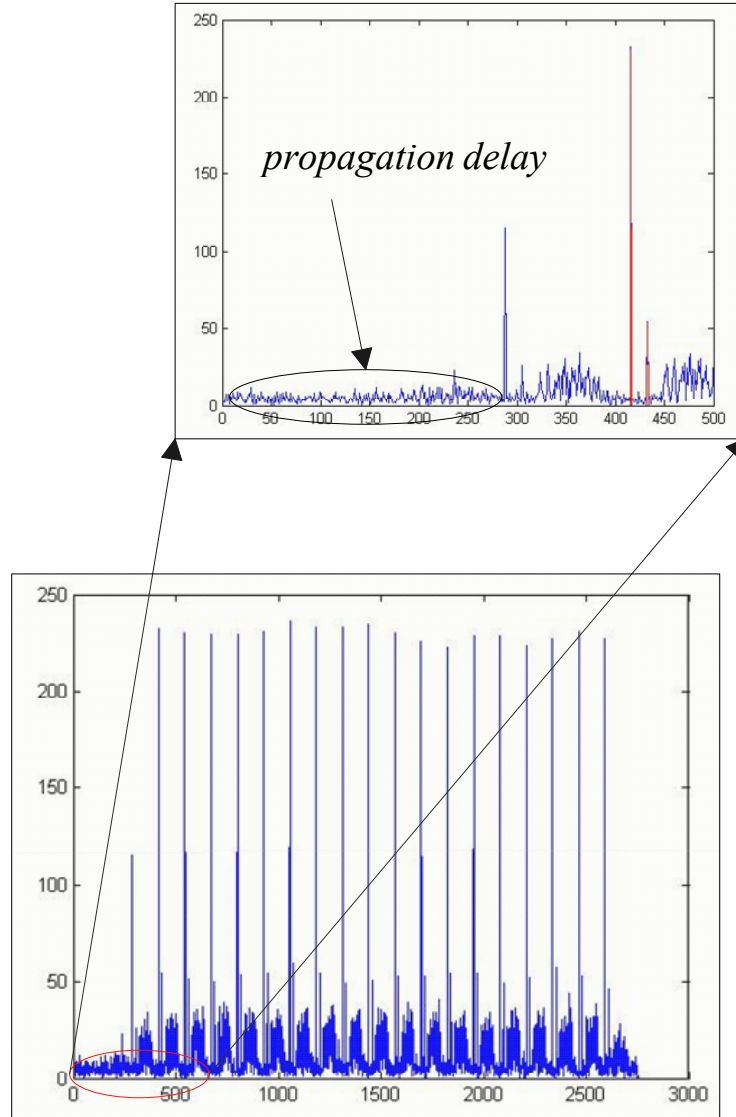
Figure 4.6a Output sequence of matched filter

Figure 4.6b Mapping the CIR on output of matched filter

However, if the strongest path is not the first path, then the symbol timing estimated may be incorrect [5]. Due to this problem, the modified synchronization method is proposed to increase the probability of tracking on the first path.

After we find the position ($n_{max\_pos}$) of the strongest path, we need to check if there is another path which is strong enough in the interval $[n_{max\_pos} - \tau_{max}, n_{max\_pos}]$ where $\tau_{max}$ is

19

the maximum delay of channel impulse response. Finally, we used the special assignment of

SFD to find the timing of synchronization sequence ends. We propose our synchronization

algorithm as table 4.1. Flow chart is shown in figure 4.7.
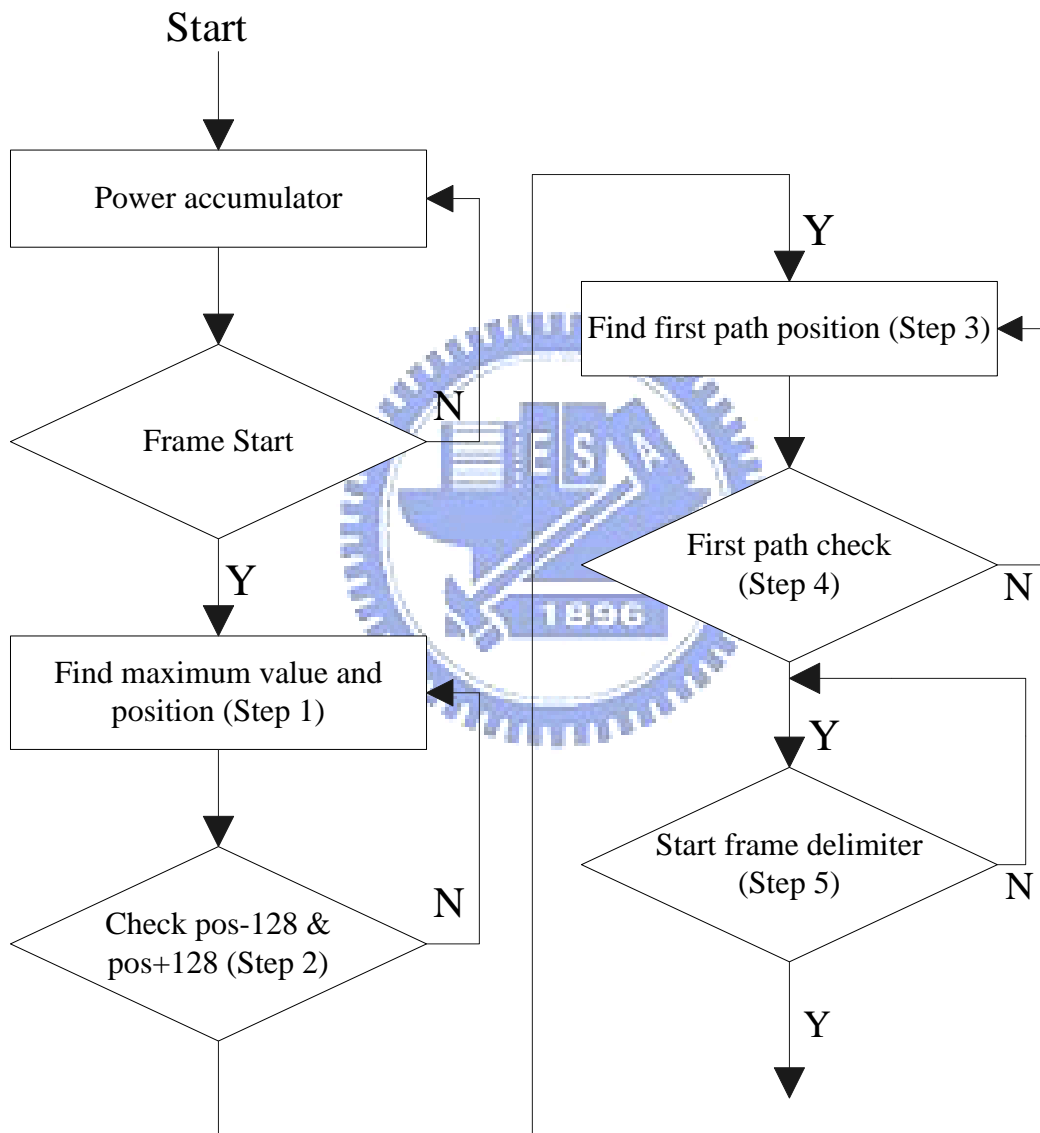


Figure 4.7 Flow chart of synchronization algorithm

**Synchronization algorithm :**

Step 1:

  find $y_{max} = \max\limits_{y(i)}\{abs(y[i])\}$

  find $n_{max\_pos} = \max\limits_{i}\{abs(y[i])\}$

Step 2:

  if $abs(y[n_{max\_pos} - 128]) > \alpha y_{max} \| abs(y[n_{max\_pos} + 128]) > \alpha y_{max}$

  $n_{first\_pos} = n_{max\_pos}$

  else

  $y[n_{max\_pos}] = 0$ and go step 1.

Step 3:

  find $y_j = y[j] \geq \gamma y_{max}$, $j$ from $n_{first\_pos} - \tau_{max}$ to $n_{first\_pos}$

  and $n_{j\_pos} = j$

Step 4:

  if $abs(y[n_{j\_pos} + 128] > \gamma y_{max}) \| abs(y[n_{j\_pos} - 128] > \gamma y_{max})$

  $n_{first\_pos} = n_{j\_pos}$.

  else

  $y[n_{j\_pos}] = 0$ and go step 3.

Step 5:

  if $(abs(y[n_{first\_pos} + 128]) < \rho y_{max})$

  *CE timing* $= n_{first\_pos} + 256$ and *Data timing* $= n_{first\_pos} + CES_{Length}$.

  else

  $n_{first\_pos} = n_{first\_pos} + 128$ and go step 5.
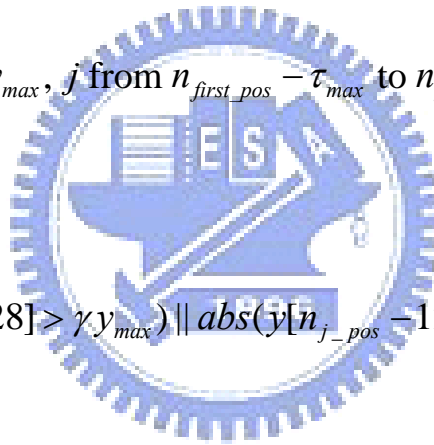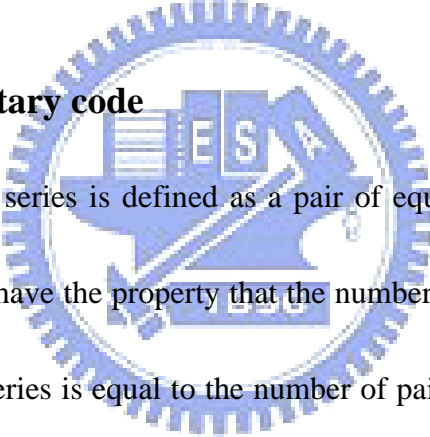
Table 4.1 Synchronization algorithm

## 4.3 Channel estimation

The issue of this section is to estimate channel impulse responses (CIRs) for later applications. We use the special structure of CES in the PLCP preamble and the correlation property of complementary sequences to develop our channel estimation scheme. Some channel estimation and channel tracking methods which use Golay complementary code for OFDM system can be found in [6] and [7]. We will introduce Golay complementary sequence first, and then we will explain our algorithm for channel estimation.

### 4.3.1  Golay complementary code

A set of complementary series is defined as a pair of equally long, finite sequences of two kinds of elements which have the property that the number of pairs of like elements with any given separation in one series is equal to the number of pairs of unlike elements with the same separation in the other series [8]. For example, the two series A=00010010 and B=0011101 are complementary.

Binary complementary code can be defined as follow. Let us consider a pair of equally long sequences $\{\alpha[n]\}$ and $\{\beta[n]\}$, for $0 \le n \le N-1$, where $N$ is the length of two sequences. These sequences are called complementary codes if their auto-correlations satisfy the relationship shown in equation 4.3.

$$\Gamma[n] \triangleq \sum_{m=0}^{N-1} \{\alpha[m]\alpha^*[((m-n))_N] + \beta[m]\beta^*[((m-n))_N]\}$$
$$= 2N\delta[n]$$
$$= \begin{cases} 2N, & n=0 \\ 0, & n \neq 0 \end{cases} \tag{4.3}$$

where $(\cdot)^*$ denotes the complex conjugate operation, and $\delta[n]$ is the Kronecker delta function. The auto-correlation of complementary sequences defined in IEEE 802.15.3c standard is shown in figure 4.8.
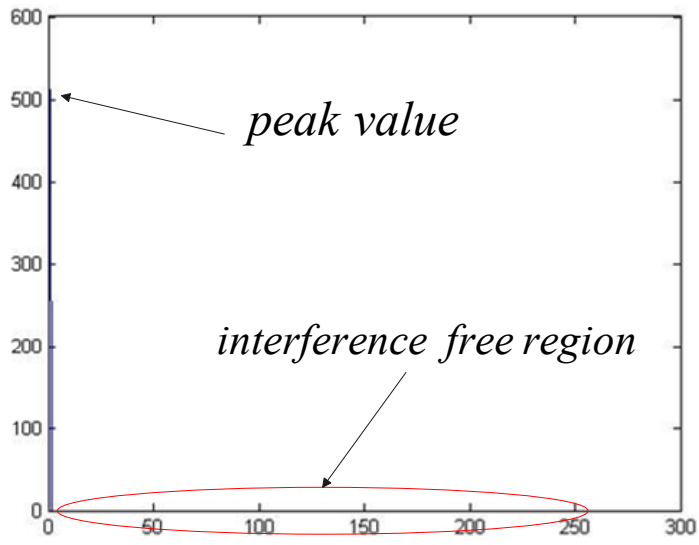


Figure 4.8 Auto-correlation of complementary codes with length 256

## 4.3.2 Channel estimation scheme

In IEEE 802.15.3c standard, the channel estimation sequence (CES) consists of one pair of complementary sequences ($a_{256}$ and $b_{256}$). Figure 4.9 shows the structure of CES, where $a_{256,pos}$, $a_{256,pre}$, $b_{256,pos}$, and $b_{256,pre}$ are the last and first half part of $a_{256}$ and $b_{256}$, respectively.

23
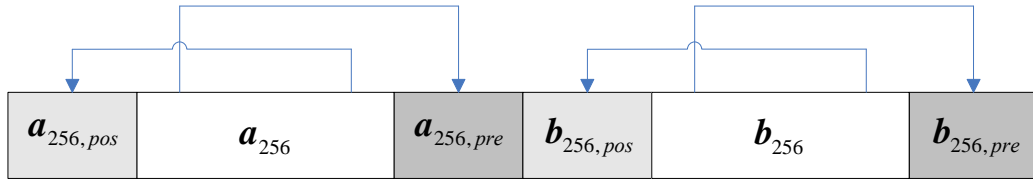
Figure 4.9 Structure of IEEE 802.15.3c SCBT CE sequence

According to this special arrangement, we can use the auto-correlation property that we introduced in the previous section to implement our channel estimation algorithm. Figure 4.10 shows a simple example for our channel estimation scheme. The received CES $r_{CE}$ is the summation of CESs with different delay arguments, gains, and phases and AWGN $n$. In this section, we assume the synchronization block can provide perfect timing for channel estimation. By using this special structure of CES, the received CES $r_{CE}$ can be represented as

$$r_{CE}[n] = \begin{cases} \sum_{l=1}^{L} a[((n-1-\tau_l))_{256}+1]\alpha_l e^{j\phi_l}, & 1 \le n \le 256 \\ \sum_{l=1}^{L} b[((n-1-512-\tau_l))_{256}+1]\alpha_l e^{j\phi_l}, & 513 \le n \le 768. \end{cases} \qquad (4.4)$$
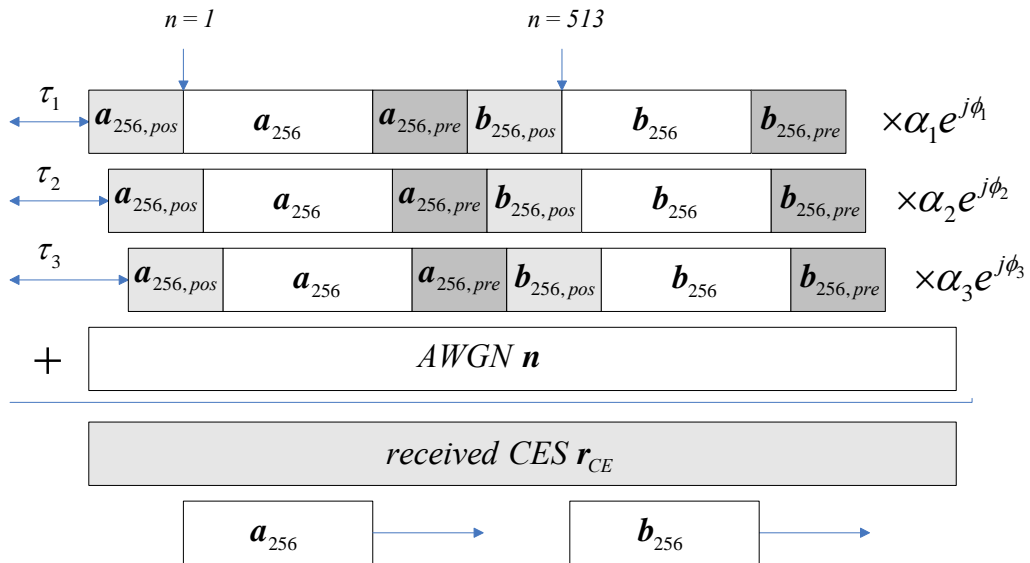


Figure 4.10 An example of channel estimation scheme

24

By using the correlation scheme (or matched filter), we can calculate the correlation between

$r_{CE}$ and $[\boldsymbol{a}_{256} \quad \underline{0}_{256} \quad \boldsymbol{b}_{256}]$. If we know the maximum channel delay which is smaller than CP

length in general, then output sequence of matched filter can be modified as

$$c[m] = \sum_{n=1}^{256} (\sum_{l=1}^{L} a[((n-1-\tau_l))_{256}+1]\alpha_l e^{j\phi_l} a[((n-1-m))_{256}+1])$$
$$+ \sum_{n=513}^{768} (\sum_{l=1}^{L} b[((n-512-\tau_l))_{256}+1]\alpha_l e^{j\phi_l} b[((n-512-m))_{256}+1])$$
$$= \sum_{l=1}^{\hat{L}} 512\hat{\alpha}_l e^{j\hat{\phi}_l} \delta[m-\hat{\tau}_l] \tag{4.5}$$

for $1 \le m \le \tau_{max}$, where $\hat{\alpha}_l$, $\hat{\phi}_l$, and $\hat{\tau}_l$ are estimated channel gain, phase, and delay, respectively.

Figure 4.11 and 4.12 show the real and the estimated channel impulse responses. We can

easily find except the original channel impulse responses, the output sequence $\{c[m]\}$ is also

affected by noise. In order to reduce the effect of noise, we develop our algorithm in table 4.2:
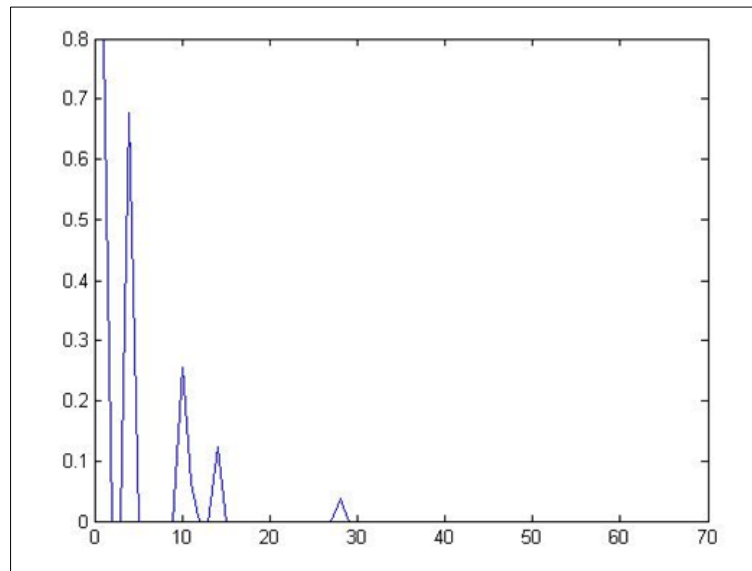


Figure 4.11 Original channel impulse responses
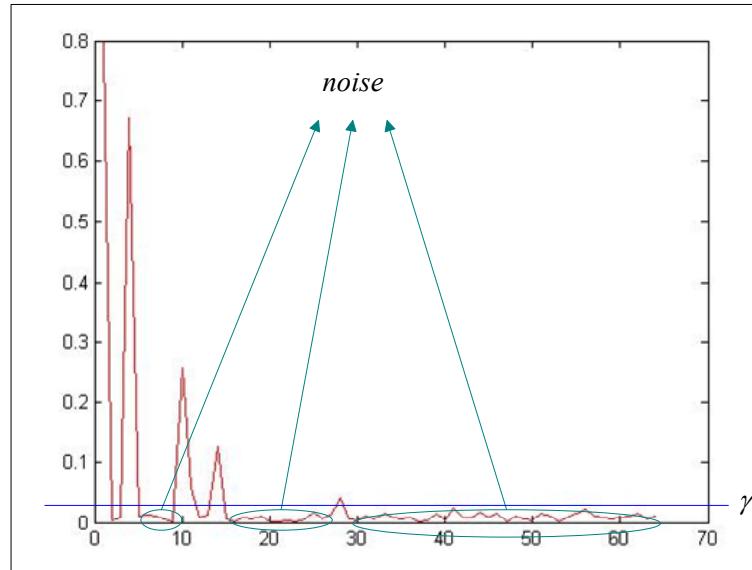
Figure 4.12 Estimated channel impulse responses with noise

**Channel estimation algorithm :**

Step 1.

Calculate $c[m]$ for $1 \le m \le$ delay maximum.

Set $\gamma_{th} = \gamma \max_{c[m]} \{abs(c[m])\}$ & path number $= 0$.

Step 2.

for $i = 1$ : delay maximum

    if $(c[i] > \gamma_{th})$

        $c[i] = c[i]/512$

        path number=path number+1

    else

        $c[i] = 0$

end

Table 4.2 Channel estimation method

Define the accepted threshold $\gamma_{th}$ can help us to filter the noise effect and estimate the more

accurate channel impulse responses.

26

After estimating the channel impulse responses by the above method, we also need to estimate the noise power for the following section. From above, we know the elements in sequence $\{c[m]\}$ their absolute values under the threshold $\gamma_{th}$ are constructed of i.i.d AWGN with zero mean and $\frac{N_0}{2}$ variance. We derive the noise statistic as follow:

Assume $n_{Ii}$ and $n_{Qi}$ are both Gaussian random variables with zero mean and $N_0/2$ variance.

$$\hat{n}_j = \sum_{i=1}^{512} c_i(n_{Ii} + jn_{Qi}) = \hat{n}_{Ij} + j\hat{n}_{Qj} \tag{4.6}$$

where $\hat{n}_{Ij} = \sum_{i=1}^{512} c_i n_{Ii}$, $\hat{n}_{Qj} = \sum_{i=1}^{512} c_i n_{Qi}$, and $c = [a_{256} \ b_{256}]^T$.

Then we calculate the mean and variance of $\hat{n}_{Ij}$, we find

$$E[\hat{n}_{Ij}] = E\left[\sum_{i=1}^{512} c_i n_{Ii}\right] = \sum_{i=1}^{512} c_i E[n_{Ii}] = 0, \tag{4.7}$$

and

$$E[\hat{n}_{Ij}^2] = E[\sum_{i=1}^{512} n_{Ii}^2 + \sum_{i=1}^{512} \sum_{k=i,k\neq i}^{512} c_i c_k n_{Ii} n_{Ik}] = 512N_0/2 = 256N_0. \tag{4.8}$$

Similarly, we find $\hat{n}_{Qj} \sim N(0, 256N_0)$.

Furthermore, the elements in complementary sequences $a_{256}$ and $b_{256}$ are either +1 or -1, so the complexity of this channel estimation scheme can be much reduced by replacing multiplication by inverter and summation. Because of this characteristic, we can reduce the complexity in circuit design and make it more suitable for high speed signal processing. Finally, we modify our scheme and show it in table 4.3.

**Channel estimation algorithm :**

Step 1:

Calculate $c[m]$ for $1 \le m \le \tau_{max}$.

Set $\gamma_{th} = \gamma \max\limits_{c[m]} \{abs(c[m])\}$, $path_{num} = 0$, and $\hat{\sigma}_n^2 = 0$

Step 2:

for $i = 1 : \tau_{max}$

   if $(c[i] > \gamma_{th})$

      $c[i] = c[i]/512$ and $path_{num} = path_{num} + 1$

   else

      $\hat{\sigma}_n^2 = \hat{\sigma}_n^2 + |c[i]|^2 / 512$ and $c[i] = 0$

end

Step 3:

$\hat{\alpha}_l e^{j\hat{\phi}_l} = c[l]$ and $\hat{\sigma}_n^2 = \hat{\sigma}_n^2 / (\tau_{max} - path_{num})$

Table 4.3 Modified channel estimation method

## 4.4 Equalization

After above two sections, we get the time of data sequence arriving, the estimated CIR, and estimated noise power. Now we need to equalize the channel effect on received data sequence caused by multipath fading channel. There are several equalization methods such as decision feedback equalizer which is proposed in [9]. However, according to the specification that published by IEEE 802.15.3c working group, we use the frequency domain equalizer (FED) to compensate the channel effect.

The SCBT with FDE is very similar to OFDM since both of them perform channel

equalization in frequency domain. Their difference is the position of IFFT operation. In SCBT with FDE, IFFT is placed in the receiver, between the equalization and data decision. The block diagram of FDE is shown in figure 4.13.

In figure 4.13, we show the block diagram of SCBT with FDE. Take the $k$-th block of the received signal as an example. After removing the CP, this $N$-length block can be written in vector form

$$\mathbf{y}_k \triangleq [y[k,0]\ y[k,1] \cdots y[k,N-1]]^{\mathrm{T}} \tag{4.9}$$

where $y[k,n]$ is the $n$-th symbol in the $k$-th data block. For simplicity, we drop the block index $k$ and the original vector becomes

$$\mathbf{y} \triangleq [y[0]\ y[1] \cdots y[N-1]]^{\mathrm{T}}. \tag{4.10}$$

$$\mathbf{W} = [W[0]\ W[1] \cdots W[N-1]]^{T}$$
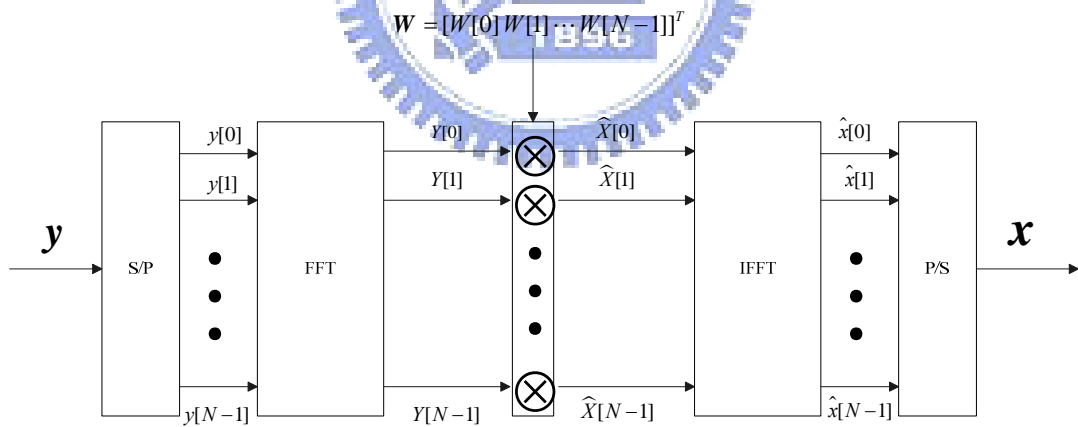


Figure 4.13 The block diagram of FDE

Through $N$-length FFT, the time domain vector $\mathbf{y}$ is transformed into frequency domain and represented as

$$\mathbf{Y} \triangleq [Y[0]\ Y[1] \cdots Y[N-1]]^{\mathrm{T}} \tag{4.11}$$

where $Y[n]$ is the signal at $n$-th subcarrier which can be expressed as

$$Y[n] = \sum_{l=0}^{N-1} y[l] \exp(-\frac{j2\pi nl}{N}). \tag{4.12}$$

Suppose the originally sent data block is

$$\boldsymbol{x} \triangleq [x[0]\, x[1] \cdots x[N-1]]^{\mathrm{T}}. \tag{4.13}$$

And its corresponding frequency domain vector is

$$\boldsymbol{X} \triangleq [X[0]\, X[1] \cdots X[N-1]]^{\mathrm{T}}. \tag{4.14}$$

Hence, the original and received frequency domain signals at the $n$-th subcarrier have the

following relationship

$$Y[n] = H[n]X[n] + N[n] \tag{4.15}$$

where $H[n]$ and $N[n]$ are channel frequency response (CFR) and noise at the $n$-th

subcarrier respectively.
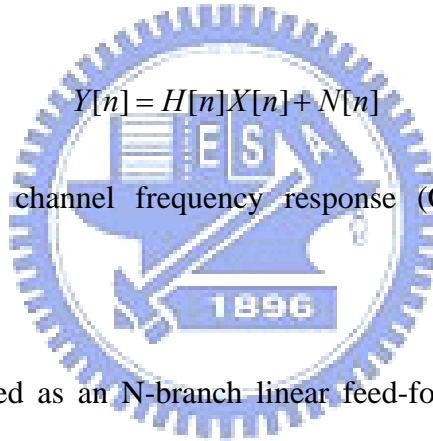
The FDE can be realized as an N-branch linear feed-forward equalizer with $W[n]$ as

complex coefficient at the $n$-th subcarrier. Transforming the equalized frequency domain

signal back into time domain by IFFT operation, we have

$$\hat{x}[n] = \frac{1}{\sqrt{N}} \sum_{l=0}^{N-1} W[l]Y[l] \exp(\frac{-j2\pi nl}{N}). \tag{4.16}$$

The equalized time domain data block

$$\hat{\boldsymbol{x}} \triangleq [x[0]\, x[1] \cdots x[n]]^{\mathrm{T}} \tag{4.17}$$

can be sent to the hard decision device for data decision or further processing.

The linear FDE can take form of either zero forcing (ZF) or minimum mean-square error

(MMSE). If optimized based on ZF criterion, the FDE coefficient $W[n]$ is

$$W_{zf}[n] = \frac{1}{H[n]}.$$ 

(4.18)

If optimized based on MMSE criterion, the FDE coefficient $W[n]$ becomes

$$W_{mmse}[n] = \frac{H^*[n]}{|H[n]|^2 + 1/\eta}$$

(4.19)

where $\eta$ denotes SNR.

In severe frequency selective fading where the spectral null (deep fading) occurs, the inversion of $H[n]$ in ZF-FDE leads to infinity and results in noise enhancement at those frequencies of spectral null. MMSE-FDE is more appealing since it can make compromise between the residual inter-symbol interference (ISI) (in the form of gain and phase mismatches) and noise enhancement. Therefore, it can minimize the combined effect of ISI and noise. This is particularly attractive for equalizing the channels of severe frequency selective fading. According to past studies, MMSE-FDE has significantly better performance than ZF-FDE for SCBT systems. However, MMSE-FDE needs to know SNR. The accuracy of SNR estimation affects the performance of MMSE-FDE [10]. The simulation result of MMSE-FDE and ZF-FDE is shown in figure 4.14.
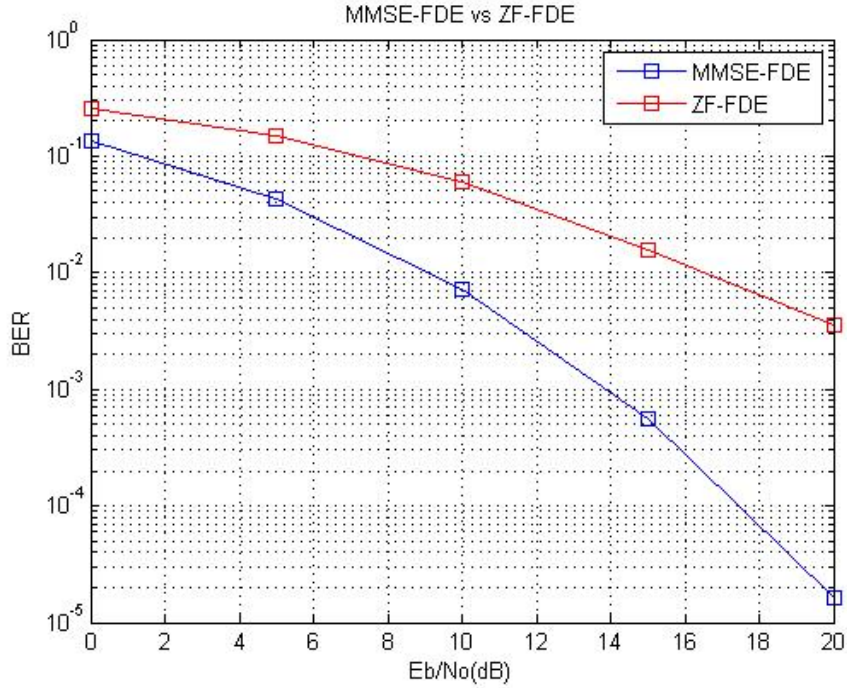
Figure 4.14 Performances of MMSE-FDE and ZF-FDE in 6-path channel

## 4.5 Data detection

In this section, we introduce some methods to improve the performance after FDE.

According to the definition of the SCBT system, the relationship between received and

transmitted signal can be written in matrix form as follow:

$$
\begin{bmatrix} y_1 \\ y_2 \\ \vdots \\ y_L \\ \vdots \\ y_N \end{bmatrix} = \begin{bmatrix} h_1 & & & h_L & \cdots & h_2 \\ h_2 & h_1 & & & \ddots & \vdots \\ \vdots & \ddots & \ddots & & & h_L \\ h_L & \ddots & \ddots & \ddots & & \\ & \ddots & \ddots & \ddots & \ddots & \\ & & h_L & \cdots & h_2 & h_1 \end{bmatrix} \begin{bmatrix} x_1 \\ x_2 \\ \vdots \\ \vdots \\ \vdots \\ x_N \end{bmatrix} + \begin{bmatrix} n_1 \\ n_2 \\ \vdots \\ \vdots \\ \vdots \\ n_N \end{bmatrix} \quad (4.20)
$$

where $y_n$, $x_n$, and $n_n$ are received signal, transmitted signal, and i.id AWGN noise

respectively.

From equation 4.20, the posteriori distribution can be expressed as

$$p(\boldsymbol{y} \mid \boldsymbol{x}) = \frac{1}{(2\pi)^{N/2}(\sigma^2)^{N/2}} \exp(-\frac{1}{2\sigma^2}(\boldsymbol{y} - H\boldsymbol{x})^H(\boldsymbol{y} - H\boldsymbol{x})). \tag{4.21}$$

In general, the best data detection performance is provided by maximum likelihood (ML) detector whose detection rule can be expressed as

$$\hat{\boldsymbol{x}}_{ML} = \max_{\boldsymbol{x}^{(i)}} p(\boldsymbol{y} \mid \boldsymbol{x}^{(i)}). \tag{4.22}$$

To maximize the conditional probability in the above equation is equivalent to minimize the following equation:

$$\hat{\boldsymbol{x}}_{ML} = \min_{\boldsymbol{x}^{(i)}}(\boldsymbol{y} - H\boldsymbol{x}^{(i)})^H(\boldsymbol{y} - H\boldsymbol{x}^{(i)}). \tag{4.23}$$

However, when the size of $\boldsymbol{x}$ becomes large, the ML detector may be too complex to be implemented in practical.

In this section, in order to focus on the data detection methods, we assume that the channel state information (CSI) is perfectly known by the receiver.

## 4.5.1 Gibbs sampler (GS)

Gibbs sampler is an application of Markov Chain Monte Carlo method which is proposed in statistics first. It is used for approaching the complex probability distribution by drawing the samples from a simple probability distribution. In other words, the Gibbs sampler is a technique for generating random variables from a marginal distribution indirectly, without having to calculate the density [11].We will introduce the Markov Chain Monte Carlo method

before we look into the Gibbs sampler in detail at later of this section.

## 4.5.1.1  Markov Chain Monte Carlo method (MCMC)

Before we mention the details of Gibbs sampler, we take a look on how a probability distribution can be approximated by generating random samples. Bayesian approach is a common method used in data detection, but usually needs high dimension of integration which is too complex to be implemented on hardware. Therefore, we introduce the Markov Chain Monte Carlo method to reduce the complexity of computation.

First, we introduce the Monte Carlo integration which is developed for high dimensional integration, the equation of Monte Carlo integration can be expressed as

$$\int_a^b h(x)dx = \int_a^b f(x)p(x)dx = E_{p(x)}[f(x)] \qquad (4.24)$$

where $p(x)$ is a probability density function defined in $[a,b]$.

As the equation mentioned above, if we draw samples $x^{(i)}$ from probability density function $p(x)$, and the number of samples is large enough. Then the integration of $h(x)$ can be expressed as

$$\int_a^b f(x)p(x)dx = E_{p(x)}[f(x)] \cong \frac{1}{N}\sum_{i=1}^N f(x^{(i)}). \qquad (4.25)$$

Moreover, we derive the conditional probability as follow:

$$\int_a^b f(y\,|\,x)p(x)dx = E_{p(x)}[f(y\,|\,x)] \cong \frac{1}{N}\sum_{i=1}^N f(y\,|\,x^{(i)}). \qquad (4.26)$$

Equation 4.24 is called Monte Carlo integration

After mentioning about Monte Carlo integration, then we introduce the Markov Chain.

We use the following equation to describe a Markov Chain process $\Pr(X_{t+1} = s_{t+1} \mid X_0 = s_0, X_1 = s_1, \cdots, X_t = s_t) = \Pr(X_{t+1} = s_{t+1} \mid X_t = s_t)$ where $X_t$ presents the sample of a variable $x$ at time $t$ and Pr is the transition probability. In other words, each sample of variable $X_{t+1}$ in Markov Chain is correlated only with the former sample $X_t$.

Now, we define the transition probability as $p(i, j) = \Pr(X_{t+1} = s_j \mid X_t = s_j)$ , and $\pi_j(t) = \Pr(X_t = s_j)$ presents the state of the Markov Chain is $s_j$ at time $t$. One important property of Markov Chain is when Markov Chain becomes stable ( $\pi_k(t + n) = \pi_k(t) = \pi_k$ for $n \geq 0$ ), then it must satisfy the detailed balance function $P_{k,j}\, \pi_k = P_{j,k}\, \pi_j$. The proof of detailed balance function is derived as

$$\pi_j = \sum_k P_{k,j}\, \pi_k = \sum_k P_{j,k}\, \pi_j = \pi_j \sum_k P_{j,k} = \pi_j. \tag{4.27}$$

## 4.5.1.2  Gibbs sampler

The Gibbs sampler was proposed by Geman in 1984 for image processing. It is a special case from Metropolis-Hastings algorithm with accepted ratio $\alpha$ always equals to 1. In other words, the samples generated by the transition probability will always be accepted. If the number of samples that we generated is large enough, then we can approach the target distribution by Monte Carlo method. The algorithm can be developed and demonstrated in table 4.4.

Given the initial values $\boldsymbol{x}^{(0)} = [x_1^{(0)}\ x_2^{(0)} \cdots\cdots\cdots x_N^{(0)}]^T$, the algorithm iterates the following loop from $n = 1$ to $n = n_0 + Ns$.

- Draw sample $x_1^{(n)}$ from $p(x_1 \mid x_2^{(n-1)}, x_3^{(n-1)} \dots, x_N^{(n-1)}, \boldsymbol{y})$.
- Draw sample $x_2^{(n)}$ from $p(x_2 \mid x_1^{(n)}, x_3^{(n-1)}, \dots, x_N^{(n-1)}, \boldsymbol{y})$.
  $$\vdots$$
- Draw sample $x_N^{(n)}$ from $p(x_N \mid x_1^{(n)}, x_2^{(n)}, \dots, x_{N-1}^{(n)}, \boldsymbol{y})$.

Samples from the last Ns iterations are used to calculate the Bayesian estimates of the unknown quantities. The initial period of length $n_0$ is known as the "burn-in" period.

$$\Rightarrow \int f(\boldsymbol{x}) p(\boldsymbol{x} \mid \boldsymbol{y}) d\underline{x} \cong \frac{1}{N} \sum_{n=n_0+1}^{n_0+Ns} f(\boldsymbol{x}^{(n)})$$

Table 4.4 General Gibbs Sampler algorithm

According to the equation 4.21 at the beginning of this section, we know that

$$p(\boldsymbol{y} \mid \boldsymbol{x}) \propto \exp(-\frac{1}{2\sigma^2}(\boldsymbol{y} - H\boldsymbol{x})^H (\boldsymbol{y} - H\boldsymbol{x})). \qquad (4.28).$$

To start the Gibbs sampler process, we need to calculate the probability density function (PDF)

$p(x_n \mid \boldsymbol{y}, x_1, \cdots, x_{n-1}, x_{n+1}, \cdots, x_N)$. As the derivation in [12], we derive target PDF as follow:

$$
\begin{aligned}
p(x_n \mid \boldsymbol{y}, x_1, \cdots, x_{n-1}, x_{n+1}, \cdots, x_N) &= \frac{p(\boldsymbol{y} \mid \boldsymbol{x}) p(\boldsymbol{x})}{p(\boldsymbol{y}, x_1, \cdots, x_{n-1}, x_{n+1}, \cdots, x_N)} \\
&= \frac{p(\boldsymbol{y} \mid \boldsymbol{x}) p(x_n)\, \overline{p(x_{1,\dots}, x_{n-1}, x_{n+1}, \cdots, x_N)}}{p(\boldsymbol{y} \mid x_{1,\dots}, x_{n-1}, x_{n+1}, \cdots, x_N)\, \overline{p(x_{1,\dots}, x_{n-1}, x_{n+1}, \cdots, x_N)}} \\
&= \frac{p(\boldsymbol{y} \mid \boldsymbol{x}) p(x_n)}{\sum_{i=1}^{M} p(\boldsymbol{y} \mid x_1, \cdots, x_{n-1}, x_n = m_i, x_{n+1}, \cdots, x_N) p(x_n = m_i)} \qquad (4.29)
\end{aligned}
$$

where $m_i$ is the possible symbol of $x_n$, and M is the total number of possible symbols of x.

If the probability $p(x_n = m_i)$ for all $i$ are equally likely which is suitable for general cases in communication engineering. Then we can continue to derive above equation as

$$p(x_n \mid \boldsymbol{y}, x_1, \cdots, x_{n-1}, x_{n+1}, \cdots, x_N) = \frac{p(\boldsymbol{y} \mid \boldsymbol{x})}{\sum_{x_n} p(\boldsymbol{y} \mid \boldsymbol{x})}. \tag{4.30}$$

For example, in BPSK transmission,

$$p(x_n = 1 \mid \boldsymbol{y}, x_1, \cdots, x_{n-1}, x_{n+1}, \cdots, x_N) = \frac{p(\boldsymbol{y} \mid \boldsymbol{x})_{x_n=1}}{\sum_{x_n} p(\boldsymbol{y} \mid \boldsymbol{x})}. \tag{4.31}$$

Then the ratio $1/D_n$ which is defined as $\dfrac{p(x_n = 1 \mid \boldsymbol{y}, x_1, \cdots, x_{n-1}, x_{n+1}, \cdots, x_N)}{p(x_n = -1 \mid \boldsymbol{y}, x_1, \cdots, x_{n-1}, x_{n+1}, \cdots, x_N)}$ can be

derived as

$$
\begin{aligned}
1/D_n &= \frac{p(x_n = 1 \mid \boldsymbol{y}, x_1, \cdots, x_{n-1}, x_{n+1}, \cdots, x_N)}{p(x_n = -1 \mid \boldsymbol{y}, x_1, \cdots, x_{n-1}, x_{n+1}, \cdots, x_N)} \\
&= \exp(-\frac{1}{2\sigma^2}(\lVert \boldsymbol{y} - H\boldsymbol{x} \rVert^2_{x_n=1} - \lVert \boldsymbol{y} - H\boldsymbol{x} \rVert^2_{x_n=-1})).
\end{aligned} \tag{4.32}
$$

After we get the above probabilities, we draw a sample $u_n$ from random variable $U$ which is

uniformly distributed in an interval $[0,1]$. And we decide the value of sample $x_n$ by

following rule:

$$x_n = \begin{cases} 1, & \text{if } u_n < \dfrac{1}{1 + D_n^{(i)}} \\ -1, & \text{Otherwise} \end{cases}. \tag{4.33}$$

According to the above derivation, we conclude our Gibbs sampler detector algorithm for

SCBT system in BPSK transmission in table 4.5.

To compute the number of multiplications in Gibbs sampler detector, we found to

calculate $\lVert \boldsymbol{y} - H\boldsymbol{x} \rVert^2_{x_n^{(i)}=1}$ need $2P$ multiplications, where $P$ is the number of paths. In general,

$2P \times M \times N$ multiplications per iteration and $2P \times M$ multiplications per symbol are

needed, where $M$ is the number of transmitted symbols, $N$ is the length of data symbols. If the

Gibbs sampler iterates $Ns$ times, there are $2P \times M \times N \times Ns$ multiplications in this process.

More detail in calculation for number of multiplications is shown in appendix A.

### Gibbs sampler algorithm (BPSK transmission)

Step 1.

Start with an initial values $\boldsymbol{x}^{(0)} = [x_1^{(0)}, x_2^{(0)}, \cdots x_N^{(0)}]^T$.

Calculate $Hx = \sum_{p=1}^{P} x^{(0)} h_p$

Step 2.

for $i = 1 \sim (n_0 + Ns)$

   for $n = 1 \sim N$

      Calculate

$$d_n = \left\| \boldsymbol{y} - H\boldsymbol{x} \right\|^2_{x_n^{(i)}=1} - \left\| \boldsymbol{y} - H\boldsymbol{x} \right\|^2_{x_n^{(i)}=-1}$$

$$= \sum_{p=1}^{P} \left( \left\| y[((n+\tau_p - 2))_N + 1] - Hx[((n+\tau_p - 2))_N + 1] + h_p(x^{(n_s-1)}[n]-1) \right\|^2 \right)$$

$$- \sum_{p=1}^{P} \left( \left\| y[((n+\tau_p - 2))_N + 1] - Hx[((n+\tau_p - 2))_N + 1] + h_p(x^{(n_s-1)}[n]+1) \right\|^2 \right)$$

      Calculate

$$\frac{p(x_n^{(i)} = 1 \mid \boldsymbol{y}, x_1^{(i)}, \cdots, x_{n-1}^{(i)}, x_{n+1}^{(i-1)}, \cdots, x_N^{(i-1)})}{p(x_n^{(i)} = -1 \mid \boldsymbol{y}, x_1^{(i)}, \cdots, x_{n-1}^{(i)}, x_{n+1}^{(i-1)}, \cdots, x_N^{(i-1)})} = \exp(-\frac{1}{2\sigma^2}(d_n)) = 1/D_n^{(i)}$$

      Draw a random value $u_n \sim U(0,1)$

$$x_n = \begin{cases} 1, & \text{if } u_n < \dfrac{1}{1+D_n^{(i)}} \\ -1, & \text{Otherwise} \end{cases}$$

   end

end

Step 3.

Take the last Ns samples $\boldsymbol{x}_{n_0+1} \sim \boldsymbol{x}_{n_0+Ns}$, and make decision by the following rule:

$$\hat{x}_i = \begin{cases} 1, & \text{if } num(x_i^n = 1) > num(x_i^n = -1) \\ -1, & \text{othrwise} \end{cases} .$$

Table 4.5 Gibbs Sampler algorithm in SCBT data detection

There are some problems need to be discussed when using Gibbs sampler in our system. One is the number of burn-in period and total samples. It would become a tradeoff between complexity and performance. The fewer samples we take the lower complexity we have, but it leads the poor performance and vice versa. In this case, we can use experience to find the best performance on the constraint of computation complexity or efficiency to solve this problem.

The other problem is the selection of initial values. The past studies had shown that the Gibbs sampler performs well in low SNR region, it may suffer from a noise floor, or even its performance may degrade as SNR increase. At high SNR region, some of the transition probabilities in the underlying Markov Chain may become very small. It leads the Markov Chain may be divided into several disjoint chains. As the result, a Gibbs sampler which starts from a random initial set will remain within the set surrounding the initial set. Then this chain may converge at local minimum and become stable [13]. To face this situation, we can use some simple method to get a set of initial values around the global optimum. Developed in our system, the result by making hard decision after FDE may be good enough to solve this problem. Figure 4.15 shows the complete block diagram of the proposed Gibbs sampler detector.
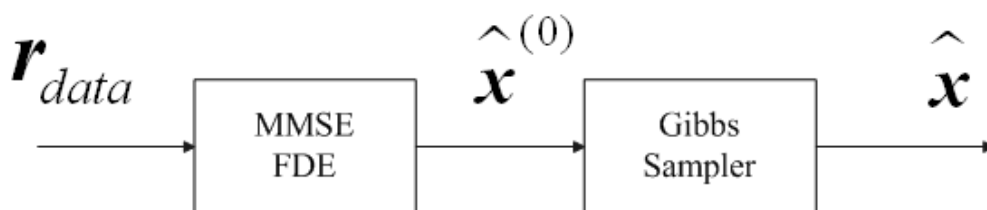


Figure 4.15 The block diagram of our Gibbs Sampler detector

## 4.5.2 Multi-path interference cancellation (MPIC)

Another method to enhance the performance in data detection is MPIC. In multi-path channel, the received signal will be interfered by other paths. The basic idea of this approach is to treat the signals from other paths as interferences. After cancelling these interferences, we do the maximum ratio combining of remaining signals to get the better performance.
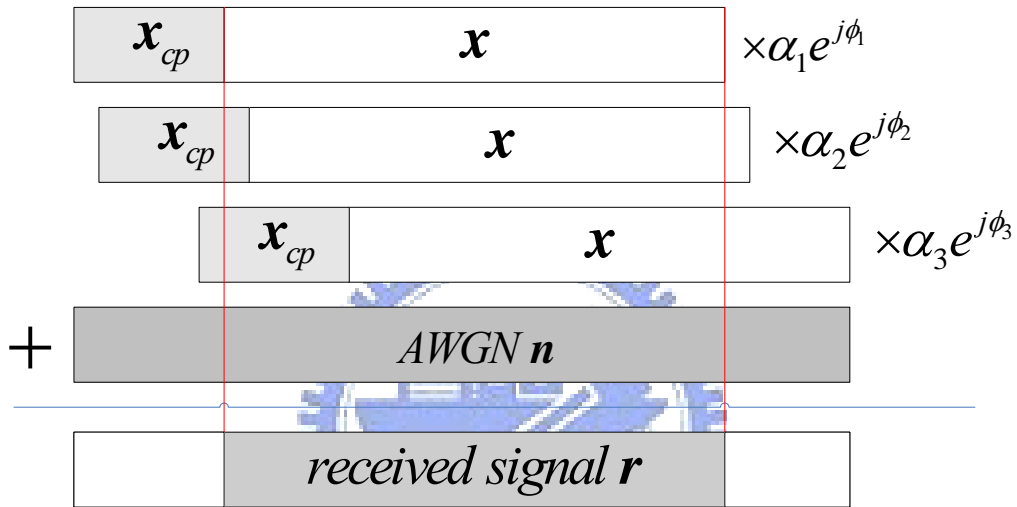


Figure 4.16 Received data signal over multipath channel

Figure 4.16 displays that the received signal $r$ is the summation of noise and the transmitted signal $x$ circular shifted by three different delay arguments, $\tau_l$, then multiplied by corresponding channel gain $\alpha_l$ and phase $\phi_l$. The received signal $r$ can be described by following equation:

$$r[n] = \sum_{l=1}^{L} x[((n-1-\tau_l))_N + 1]\alpha_l e^{j\phi_l} + n_n, \qquad 1 \le n \le N. \qquad (4.34)$$

From section 4.4, after equalization the ISI which caused by multipath channel, we can get a set of estimated $x$, named $\hat{x}^{(0)}$. By using this $\hat{x}^{(0)}$ as the initial value of MPIC

method, we can reconstruct a received signal $\hat{r}$ which can be written as

$$\hat{r}[n] = \sum_{l=1}^{L} \hat{x}[((n-1-\tau_l))_N + 1]\alpha_l e^{j\phi_l}, \qquad 1 \le n \le N. \qquad (4.35)$$

Then we define $\hat{r}_i$ which is $\hat{r}$ subtracted the component of the i-th path, the formula of $\hat{r}_i$

is represented as

$$\hat{r}_i[n] = \sum_{\substack{l=1 \\ l \ne i}}^{L} \hat{x}[((n-1-\tau_l))_N + 1]\alpha_l e^{j\phi_l} = \hat{r}[n] - \hat{x}[((n-1-\tau_i))_N + 1]\alpha_i e^{j\phi_i}, \quad 1 \le n \le N. \quad (4.36)$$

Then the estimated signal from the i-th path which defined as $\hat{x}_i$ can be expressed as

$$
\begin{aligned}
\hat{x}_i[((n-1-\tau_i))_N + 1] &= r[n] - \hat{r}_i[n] \\
&= \sum_{l=1}^{L} x[((n-1-\tau_l))_N + 1]\alpha_l e^{j\phi_l} + n_n - \sum_{\substack{l=1 \\ l \ne i}}^{L} \hat{x}[((n-1-\tau_l))_N + 1]\alpha_l e^{j\phi_l} \\
&= x[((n-1-\tau_i))_N + 1]\alpha_i e^{j\phi_i} \\
&\quad + \sum_{\substack{l=1 \\ l \ne i}}^{L} (x[((n-1-\tau_l))_N + 1] - \hat{x}[((n-1-\tau_l))_N + 1])\alpha_l e^{j\phi_l} + n_n. \qquad (4.37)
\end{aligned}
$$

After we get all $\hat{x}_i[n]$ from all paths, then we can detect the $\hat{x}[n]$ by using maximum ratio

combining to combine all components from every path. The relationship between $\hat{x}_{new}[n]$

and $\hat{x}_i[n]$ can be represented as

$$
\begin{aligned}
\hat{x}_{new}[n] &= \sum_{i=1}^{L} \hat{x}_i[n]\alpha_i e^{-j\phi_i} \\
&= \sum_{i=1}^{L} \{ x[n]|\alpha_i|^2 + \sum_{\substack{l=1 \\ l \ne i}}^{L} (x[((n-1-\tau_l+\tau_i))_N + 1] - \hat{x}[((n-1-\tau_l+\tau_i))_N + 1])\alpha_l \alpha_i e^{j(\phi_l-\phi_i)} + n_n \alpha_i e^{-j\phi_i} \} \\
&= \underbrace{x[n]\sum_{i=1}^{L} |\alpha_i|^2}_{desire\ x} + \underbrace{\sum_{i=1}^{L} \sum_{\substack{l=1 \\ l \ne i}}^{L} (x[((n-1-\tau_l+\tau_i))_N + 1] - \hat{x}[((n-1-\tau_l+\tau_i))_N + 1])\alpha_l \alpha_i e^{j(\phi_l-\phi_i)}}_{interference} \\
&\quad + \underbrace{n_n \sum_{i=1}^{L} \alpha_i e^{-j\phi_i}}_{noise}. \qquad (4.38)
\end{aligned}
$$

When $\hat{x}[n]$ is very similar to the transmitted signal $x[n]$, the interference term in equation 4.38 would be small enough. As a result, we can make the decision from $\hat{x}_{new}[n]$ directly. Then we take $\hat{x}_{new}[n]$ as $\hat{x}[n]$ in equation 4.38 and start it all over again. After iterations, we expect $\hat{x}[n]$ will converge to more accurate solution. We propose the MPIC detector algorithm in table 4.6.

**MPIC algorithm :**

Step 1:

Start from given initial value $\boldsymbol{x}^{(0)} = [x_1^{(0)}\ x_2^{(0)}\ \cdots\cdots\cdots x_N^{(0)}]^T$ which provided by FDE.

Step 2:

for $k = 1 : Ns$

$$\hat{r}^{(k)}[n] = \sum_{l=1}^{L} \hat{x}^{(k-1)}[((n-1-\tau_l))_N + 1]\alpha_i e^{j\phi_l}, \qquad 1 \le n \le N$$

    for $i = 1 : path_{num}$

$$\hat{r}_i^{(k)}[n] = \hat{r}^{(k)}[n] - \hat{x}^{(k-1)}[((n-1-\tau_i))_N + 1]\alpha_i e^{j\phi_i}, \qquad 1 \le n \le N$$

$$\hat{x}_i^{(k)}[((n-1-\tau_i))_N + 1] = r[n] - \hat{r}_i^{(k)}[n], \qquad 1 \le n \le N$$

    end

$$\hat{x}^{(k)}[n] = \sum_{i=1}^{L} \hat{x}_i^{(k)}[n]\alpha_i e^{-j\phi_i}, \qquad\qquad 1 \le n \le N$$

end

Step 3:

Take the $\hat{x}^{(Ns)}$ as the final solution of $\boldsymbol{x}.$

Table 4.6 MPIC detector method in SCBT system

From simulation results in the next chapter, we found an important issue for using this method. The selection of the initial value affects the system performance seriously. The bad

starting point may let performance become worse during iterations.

To calculate the computation complexity of MPIC detector, we need $P \times N$ multiplications in total to compute the estimated received signal from each path. Then we use other $P \times N$ multiplications for maximal ratio combining signals, where $P$ is the number of paths and $N$ is the length of a data block. To summarize, we need $2 \times P \times N$ multiplications in total per iteration. In other words, only $2 \times P$ multiplications are needed for a data symbol in iteration. For example, if the MPIC detector iterates $Ns$ times, there are $2 \times P \times N \times Ns$ multiplications in this process. Figure 4.17 shows the complete block diagram of the proposed MPIC detector.
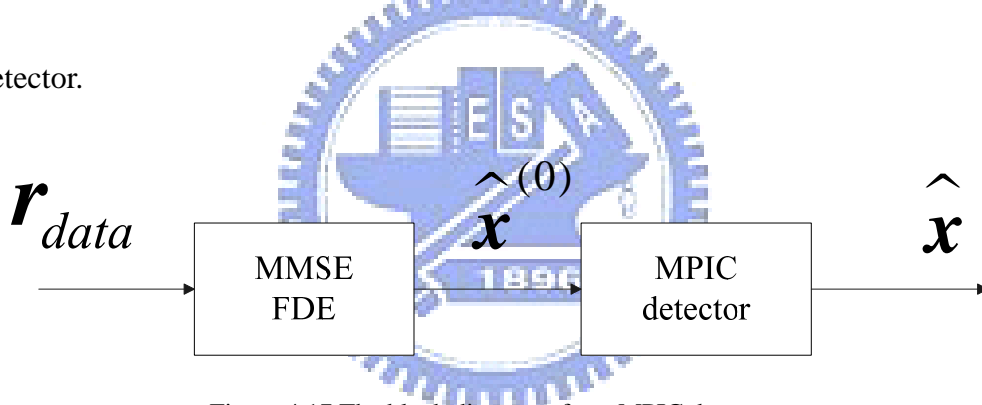


Figure 4.17 The block diagram of our MPIC detector

## 4.5.3 Probabilistic data association (PDA)

A Probabilistic Data Association (PDA) method is proposed for multiuser detection over synchronous code-division multiple access (CDMA) communication channels. The performance of this method in [14] shows that it is very close to the optimal maximum likelihood (ML) detector. Because the ML bound in our system seems impossible to find, we use the PDA method to approach the ML bound. And compare the performances of the

detectors we proposed with PDA method together.

Base on SCBT system, the PDA algorithm for circular convolution channel is introduced in [15]. PDA models the undecided signals as random variable. For example, in BPSK transmission, the signals will be modeled as binary random variables. By approximating the inter-symbol interference as Gaussian noise with appropriately elevated covariance matrix, the probability associated with each transmitted signal is iteratively updated. Computer simulation shows that probabilities usually converge within two or three iterations, and the performance of this algorithm is very close to sphere decoding (SD) algorithm [16].

In the SCBT system with BPSK transmission, we treat each data symbol as a binary random variable. For $x_i$, we associate a probability $p_b(i)$ which means the current estimated probability of $x_i = 1$. $p_b(i)$ can be defined in mathematical form as

$$p_b(i) = p(x_i = 1 \mid \boldsymbol{y}, \{p_b(j)\}_{j \neq i}). \tag{4.39}$$

Similarly, $1 - p_b(i)$ is corresponding to the current estimated probability of $x_i = -1$,

$$p(x_i = -1 \mid \boldsymbol{y}, \{p_b(j)\}_{j \neq i}). \tag{4.40}$$

From equation 4.20, we have the relationship between transmitted and received signals. We modify the equation 4.20 as follow:

$$\begin{bmatrix} y_1 \\ y_2 \\ \vdots \\ y_N \end{bmatrix} = \begin{bmatrix} \boldsymbol{h}_1 & \boldsymbol{h}_2 & \cdots & \boldsymbol{h}_N \end{bmatrix} \begin{bmatrix} x_1 \\ x_2 \\ \vdots \\ x_N \end{bmatrix} + \begin{bmatrix} n_1 \\ n_2 \\ \vdots \\ n_N \end{bmatrix} \Rightarrow \boldsymbol{y} = \boldsymbol{h}_i x_i + \underbrace{\sum_{j=1, j \neq i}^{N} \boldsymbol{h}_j x_j + \boldsymbol{n}}_{N_i}. \tag{4.41}$$

Now, we treat other data symbol $x_j \ (j \neq i)$ as binary random variables and treat

$\sum_{j=1, j \neq i}^{N} \boldsymbol{h}_j x_j + \boldsymbol{n}$ as a Gaussian random vector $N_i$ which means $\boldsymbol{N}_i \sim N(\boldsymbol{\mu}_i, \Sigma_i)$.

Base on our assumption, we need to calculate mean vector $\boldsymbol{\mu}_i$ and covariance matrix $\Sigma_i$ of $N_i$. We derive $\boldsymbol{\mu}_i$ and $\Sigma_i$ below:

$$
\begin{aligned}
\boldsymbol{\mu}_i = E[\boldsymbol{N}_i] = E[\sum_{j=1, j \neq i}^{N} \boldsymbol{h}_j x_j] + E[\boldsymbol{n}] = \sum_{j=1, j \neq i}^{N} \boldsymbol{h}_j E[x_j] \\
= \sum_{j=1, j \neq i}^{N} \boldsymbol{h}_j p_b(j) - \boldsymbol{h}_j(1 - p_b(j)) = \sum_{j=1, j \neq i}^{N} \boldsymbol{h}_j(2 p_b(j) - 1),
\end{aligned}
\tag{4.42}
$$

and

$$
\begin{aligned}
\Sigma_i &= \mathrm{var}(\boldsymbol{N}_i) = E[\boldsymbol{N}_i \boldsymbol{N}_i^H] - E^2[\boldsymbol{N}_i] \\
&= \sum_{j=1, j \neq i}^{N} \sum_{k=1, k \neq i}^{N} \boldsymbol{h}_j \boldsymbol{h}_k^H E[x_j x_k] + E[\boldsymbol{n}\boldsymbol{n}^H] - \sum_{j=1, j \neq i}^{N} \sum_{k=1, k \neq i}^{N} \boldsymbol{h}_j \boldsymbol{h}_k^H (2 p_b(j) - 1)(2 p_b(k) - 1) \\
&= \sum_{j=1, j \neq i}^{N} \boldsymbol{h}_j \boldsymbol{h}_j^H E[x_j^2] + \sum_{\substack{j=1, j \neq i \\ j \neq k}}^{N} \sum_{k=1, k \neq i}^{N} \boldsymbol{h}_j \boldsymbol{h}_k^H E[x_j] E[x_k] + \sigma_n^2 I_N \\
&\quad - \sum_{j=1, j \neq i}^{N} \boldsymbol{h}_j \boldsymbol{h}_j^H (2 p_b(j) - 1)^2 + \sum_{\substack{j=1, j \neq i \\ j \neq k}}^{N} \sum_{k=1, k \neq i}^{N} \boldsymbol{h}_j \boldsymbol{h}_k^H (2 p_b(j) - 1)(2 p_b(k) - 1) \\
&= \sum_{j=1, j \neq i}^{N} \boldsymbol{h}_j \boldsymbol{h}_j^H 4 p_b(j)(1 - p_b(j)) + \sigma_n^2 I_N
\end{aligned}
\tag{4.43}
$$

where $\sigma_n^2$ is the variance of AWGN noise, and $I_N$ is an $N \times N$ identity matrix. From equation 4.41, we know that $\boldsymbol{y} - \boldsymbol{h}_i x_i \sim N(\boldsymbol{\mu}_i, \Sigma_i)$. According to above deriving, we have

$$
\begin{aligned}
p_b(i) &= p(x_i = 1 \mid \boldsymbol{y}, \{p_b(j)\}_{j \neq i}) \\
&= \frac{1}{(2\pi)^{N/2} |\Sigma_i|^{1/2}} \exp(-\frac{1}{2}(\boldsymbol{y} - \boldsymbol{h}_i - \boldsymbol{\mu}_i)^H \Sigma_i^{-1}(\boldsymbol{y} - \boldsymbol{h}_i - \boldsymbol{\mu}_i)),
\end{aligned}
\tag{4.44}
$$

and

$$
\begin{aligned}
1 - p_b(i) &= p(x_i = -1 \mid \boldsymbol{y}, \{p_b(j)\}_{j \neq i}) \\
&= \frac{1}{(2\pi)^{N/2} |\Sigma_i|^{1/2}} \exp(-\frac{1}{2}(\boldsymbol{y} + \boldsymbol{h}_i - \boldsymbol{\mu}_i)^H \Sigma_i^{-1}(\boldsymbol{y} + \boldsymbol{h}_i - \boldsymbol{\mu}_i)).
\end{aligned}
\tag{4.45}
$$

From equation 4.44 and equation 4.45, we get the ratio

$$\frac{p_b(i)}{1-p_b(i)} = \frac{\exp(-\frac{1}{2}(y-h_i-\mu_i)^H \Sigma_i^{-1}(y-h_i-\mu_i))}{\exp(-\frac{1}{2}(y+h_i-\mu_i)^H \Sigma_i^{-1}(y+h_i-\mu_i))}$$

$$= \exp(-\frac{1}{2}((y-\mu_i)-h_i)^H \Sigma_i^{-1}((y-\mu_i)-h_i)) - \exp(-\frac{1}{2}((y-\mu_i)+h_i)^H \Sigma_i^{-1}((y-\mu_i)+h_i))$$

$$= \exp(-\frac{1}{2}(y-\mu_i)^H \Sigma_i^{-1}(y-\mu_i) + \frac{1}{2}(y-\mu_i)^H \Sigma_i^{-1}h_i + \frac{1}{2}h_i^H \Sigma_i^{-1}(y-\mu_i) - \frac{1}{2}h_i^H \Sigma_i^{-1}h_i$$

$$+ \frac{1}{2}(y-\mu_i)^H \Sigma_i^{-1}(y-\mu_i) + \frac{1}{2}(y-\mu_i)^H \Sigma_i^{-1}h_i + \frac{1}{2}h_i^H \Sigma_i^{-1}(y-\mu_i) + \frac{1}{2}h_i^H \Sigma_i^{-1}h_i)$$

$$= \exp(\frac{1}{2}\{(y-\mu_i)^H \Sigma_i^{-1}h_i + h_i^H \Sigma_i^{-1}(y-\mu_i) + (y-\mu_i)^H \Sigma_i^{-1}h_i + h_i^H \Sigma_i^{-1}(y-\mu_i)\})$$

$$= \exp(2\,\mathrm{Re}\{(y-\mu_i)^H \Sigma_i^{-1}h_i\}). \tag{4.46}$$

It can easily be seen that the desire probability $p_b(i)$ is

$$p_b(i) = \frac{1}{1+\exp(-2\,\mathrm{Re}\{(y-\mu_i)^H \Sigma_i^{-1}h_i\})}. \tag{4.47}$$

After a few iterations, the probability $p_b(i)$ will converge to the stable value. Then we can

make decision by following rule:

$$x_i = \begin{cases} 1, & if\ p_b(i) \geq 0.5 \\ -1, & if\ p_b(i) < 0.5 \end{cases}. \tag{4.48}$$

Base on these equations, the basic form of the proposed PDA detector is as follow:

**PDA algorithm :**

Step 1.

set $p_b(i) = 0.5$ for $i = 1 \sim N$, and $\boldsymbol{\mu} = \mathbf{0}$, $\Sigma = HH^H + \sigma_n^2 I_N$.

where $\boldsymbol{\mu} = \boldsymbol{\mu}_i + (2p_b(i) - 1)\boldsymbol{h}_i$, $\Sigma = \Sigma_i + 4p_b(i)(1 - p_b(i))\boldsymbol{h}_i\boldsymbol{h}_i^H$

Step 2.

for $k = 2 \sim Ns$

    for $i = 1 \sim N$

$$\boldsymbol{\mu}_i = \boldsymbol{\mu} - (2p_b^{(k-1)}(i) - 1)\boldsymbol{h}_i,$$

$$\Sigma_i^{-1} = (\Sigma - 4p_b^{(k-1)}(i)(1 - p_b^{(k-1)}(i))\boldsymbol{h}_i\boldsymbol{h}_i^H)^{-1}$$

$$= \Sigma^{-1} + \frac{4p_b^{(k-1)}(i)(1 - p_b^{(k-1)}(i))\Sigma^{-1}\boldsymbol{h}_i\boldsymbol{h}_i^H\Sigma^{-1}}{1 - 4p_b^{(k-1)}(i)(1 - p_b^{(k-1)}(i))\boldsymbol{h}_i^H\Sigma^{-1}\boldsymbol{h}_i}$$

calculate $p_b^{(k)}(i) = \dfrac{1}{1 + \exp(-2\operatorname{Re}\{(\boldsymbol{y} - \boldsymbol{\mu}_i)^H\Sigma_i^{-1}\boldsymbol{h}_i\})}$

$$\boldsymbol{\mu} = \boldsymbol{\mu}_i + (2p_b^{(k)}(i) - 1)\boldsymbol{h}_i$$

$$\Sigma^{-1} = (\Sigma_i + 4p_b^{(k)}(i)(1 - p_b^{(k)}(i))\boldsymbol{h}_i\boldsymbol{h}_i^H)^{-1}$$

$$= \Sigma_i^{-1} - \frac{4p_b^{(k)}(i)(1 - p_b^{(k)}(i))\Sigma_i^{-1}\boldsymbol{h}_i\boldsymbol{h}_i^H\Sigma_i^{-1}}{1 - 4p_b^{(k)}(i)(1 - p_b^{(k)}(i))\boldsymbol{h}_i^H\Sigma_i^{-1}\boldsymbol{h}_i}$$

    end

end

Step 3.

after Ns iterations, $\hat{x}_i = \operatorname{sign}(p_b^{(Ns)}(i) - 0.5)$.

Table 4.7 PDA algorithm

The matrix inversion in step 2 is represented by the form of matrix inversion lemma (Sherman-Morrison-Woodbury formula). By using this lemma, we can reduce the number of multiplications for matrix inversion form $O(N^3)$ to $O(N^2)$. However, the computational

47

complexity of PDA algorithm is still too large in practice.

Compare the PDA method with the SD which is the method reducing the complexity of

ML detection in figure 4.18 and figure 4.19, we find that the performance of PDA is quite

close to the SD. We take the PDA method as a reference performance of our SCBT system.

| Modulation type | BPSK |
|---|---|
| FFT size | 32/64 |
| CPPS length | 8/16 |
| Channel model | 2-path & 6-path fading channel |
| Channel power profile | [0 -3] & [0 -1 -9 -10 -15 -20] |

Table 4.8 Simulation Parameters
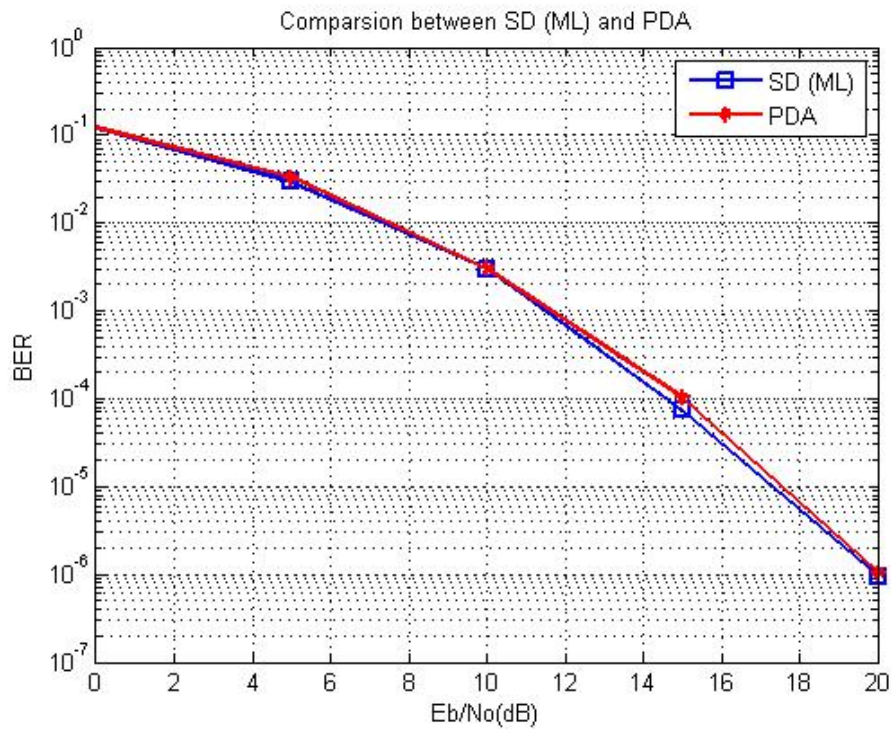


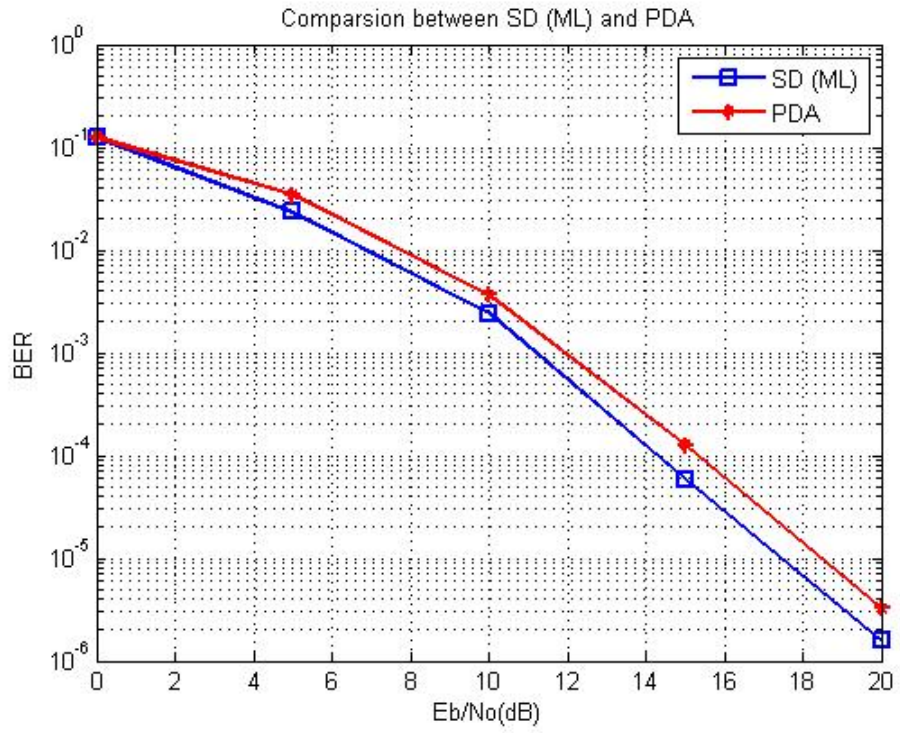Figure 4.18 Performances of SD and PDA for FFT size=32

48

Figure 4.19 Performances of SD and PDA for FFT size=64

# Chapter 5 Simulation results

In this chapter, we will show the computer simulation results for each part of the SCBT baseband receiver we proposed including synchronization, channel estimation, frequency domain equalization, and data detection. Based on these results, we make some analysis of the system performance as well.

## 5.1 Simulation results of synchronization

We use the short preamble which is defined in IEEE 802.15.3c SCBT system standard for our simulation. Table 5.1 and 5.2 show the two multipath fading channel models (2-path and 6-path) that we used. From figure 5.1 and 5.3, we know the distribution (probability) of the strongest path appears in each path index. The performances of synchronization algorithm in two channel models are shown in figure 5.2 and 5.4, where the probability is defined as the estimated symbol timing is outside the ISI free region. Furthermore, according to different threshold $\gamma$ in table 4.1, the probability of tracking on each path is shown in table 5.2 and 5.4. From the results, we can easily discover that the method we proposed for synchronization effectively improves the probability of tracking on the first path.

| Preamble type | Short |
|---|---|
| Channel model | 2-path fading channel |
| Channel power profile | [0 -3] |

Table 5.1 Parameters for synchronization in 2-path fading channel
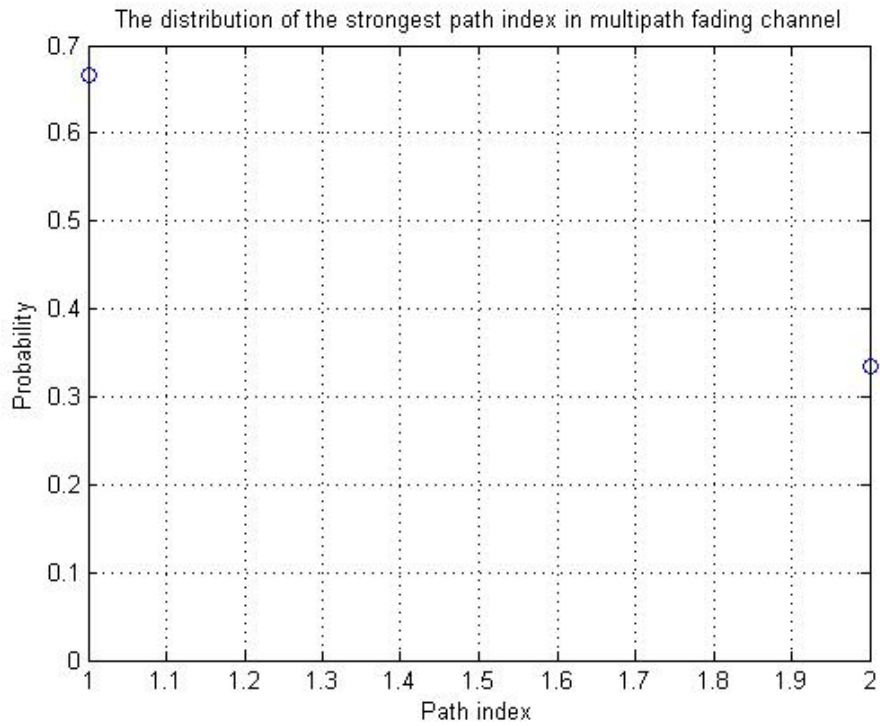
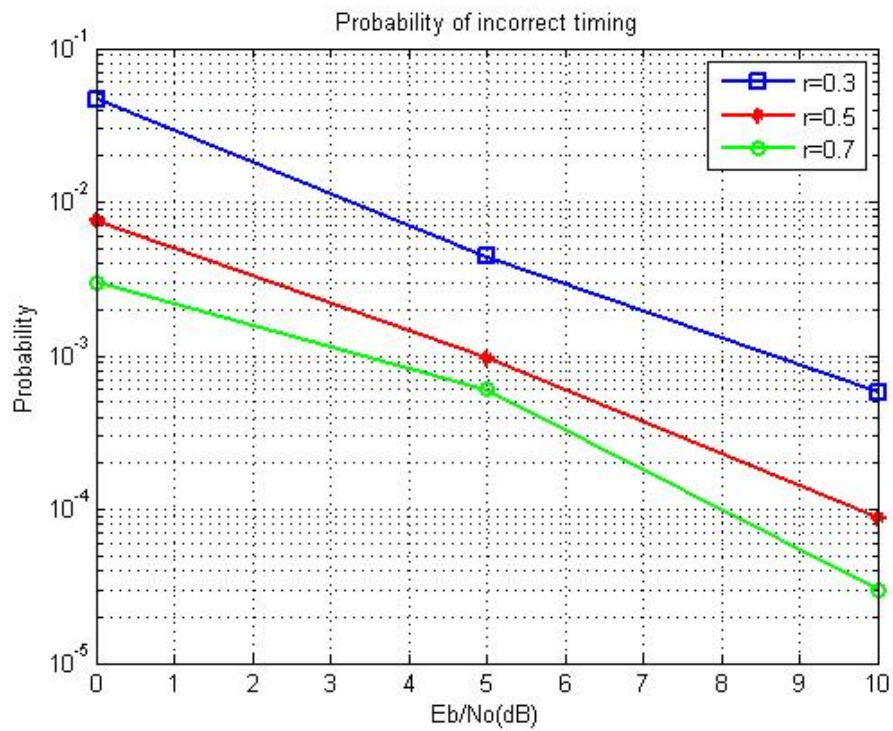Figure 5.1 Distribution of the strongest path in 2-path fading channel



Figure 5.2 Probability of synchronization error for 2-path model

50

| SNR | 0 dB | | | 5 dB | | | 10 dB | | |
|---|---|---|---|---|---|---|---|---|---|
| Threshold (γ) | γ=0.3 | γ =0.5 | γ=0.7 | γ=0.3 | γ=0.5 | γ=0.7 | γ=0.3 | γ=0.5 | γ=0.7 |
| 1 | 89.60 | 85.79 | 73.60 | 94.61 | 87.32 | 77.99 | 95.25 | 88.09 | 78.91 |
| 2 | 5.40 | 13.43 | 26.10 | 4.93 | 12.58 | 21.95 | 4.84 | 11.91 | 21.09 |

(%)

Table 5.2 Probability of tracking on each path as the first path for different γ

| Preamble type | Short |
|---|---|
| Channel model | 6-path fading channel |
| Channel power profile | [0 -1 -9 -10 -15 -20] |

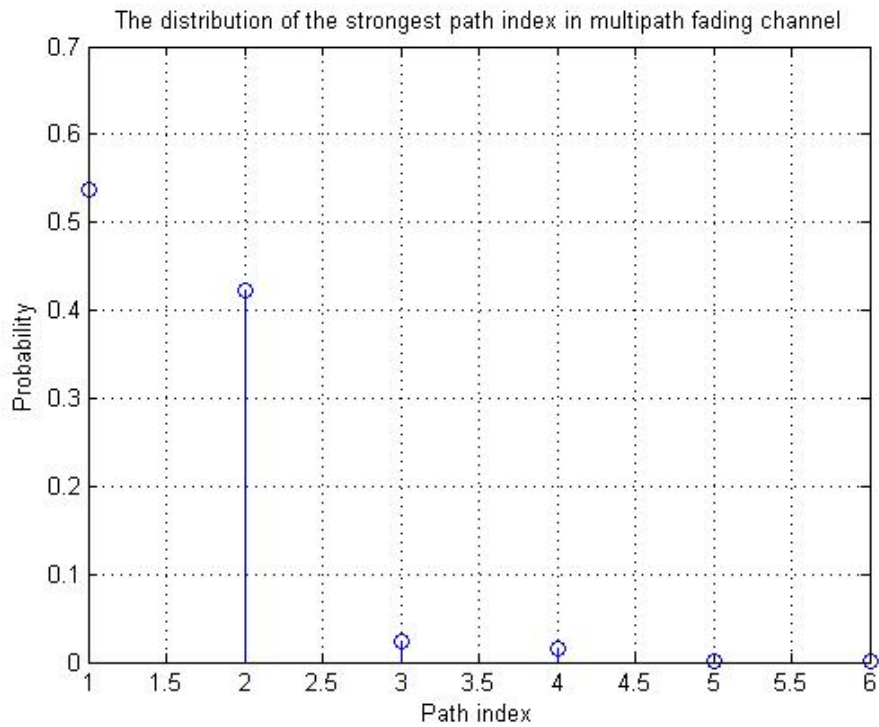Table 5.3 Parameters for synchronization in 6-path fading channel



Figure 5.3 Distribution of the strongest path in 6-path fading channel
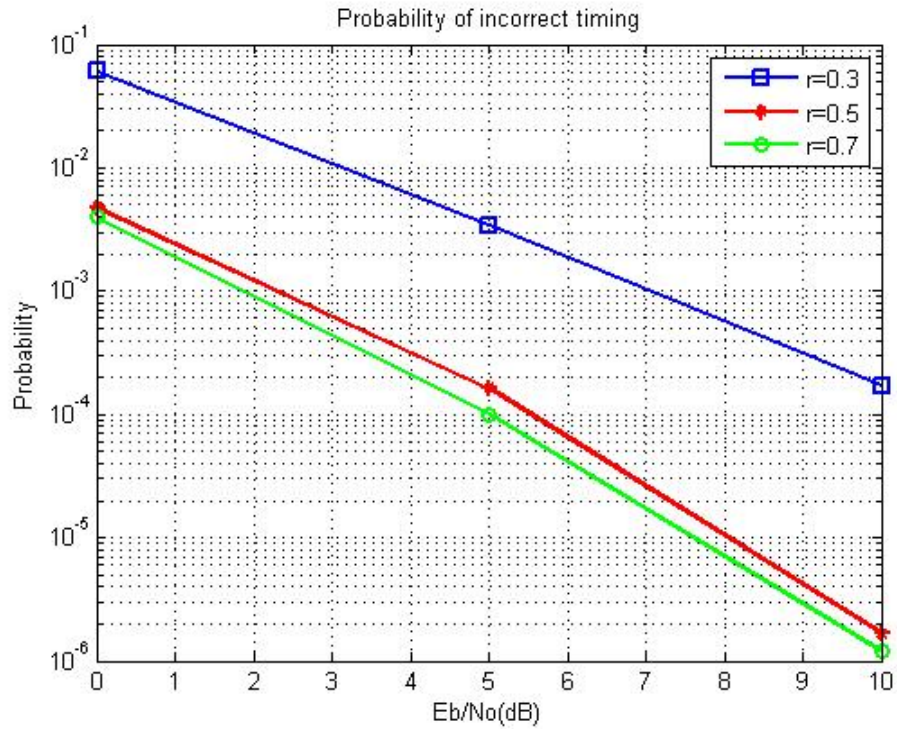
Figure 5.4 Probability of synchronization error for 6-path model

| SNR | 0 dB | | | 5 dB | | | 10 dB | | |
|---|---|---|---|---|---|---|---|---|---|
| Threshold (γ) | γ=0.3 | γ=0.5 | γ=0.7 | γ=0.3 | γ=0.5 | γ=0.7 | γ=0.3 | γ=0.5 | γ=0.7 |
| 1 | 85.40 | 79.31 | 64.90 | 92.44 | 80.94 | 67.10 | 92.60 | 81.77 | 69.10 |
| 2 | 8.10 | 19.56 | 32.10 | 7.15 | 18.54 | 30.99 | 7.32 | 17.81 | 29.44 |
| 3 | 0 | 0.47 | 2.00 | 0.06 | 0.41 | 1.29 | 0.06 | 0.33 | 1.00 |
| 4 | 0.10 | 0.15 | 0.60 | 0.01 | 0.10 | 0.58 | 0.01 | 0.10 | 0.44 |
| 5 | 0.10 | 0 | 0 | 0 | 0 | 0.03 | 0 | 0 | 0.02 |
| 6 | 0 | 0 | 0 | 0 | 0 | 0 | 0 | 0 | 0 |

(%)

Table 5.4 Probability of tracking on each path as the first path for different γ

## 5.2 Simulation results of channel estimation

Table 5.5 shows the simulation parameters for channel estimation. Figure 5.5 and 5.6 illustrate the normalized mean square errors of estimated channel impulse responses and noise power for 2-path fading channel respectively. We can know that based on different $\gamma$ in table 4.3, the mean square errors are also different with SNR. When $\gamma = 0.01$, the mean square error decreases linearly with SNR increasing.

| Modulation type | BPSK, QPSK, 16QAM, and 64QAM |
| --- | --- |
| Symbol/chip rate | 1728Mcps |
| FFT size | 256 |
| CPPS length | 64 |
| Channel model | 2-path & 6-path fading channel |
| Channel power profile | [0 -3] & [0 -1 -9 -10 -15 -20] |

Table 5.5 Simulation parameters

The performances with different modulations, form figure 5.7 to 5.10, show the BER after FDE which use the estimated CSIs for equalization in 2-path channel. The results show the performances are almost the same as the performances that use the perfect CSIs when we set $\gamma = 0.01$.

Figure 5.11 and 5.12 show the normalized mean square errors of estimated channel impulse responses and noise power for 6-path fading channel respectively. Figure 5.13 to 5.16 show the BERs after FDE which use the estimated CSIs for different type modulations in 6-path channel. As well as the case in 2-path channel, the results also show the performances

are almost the same to the performances that use the perfect CSIs when $\gamma = 0.01$. But the

degradation in BER of the inaccurate CSIs ($\gamma = 0.3$) is more serious than in 2-path channel.
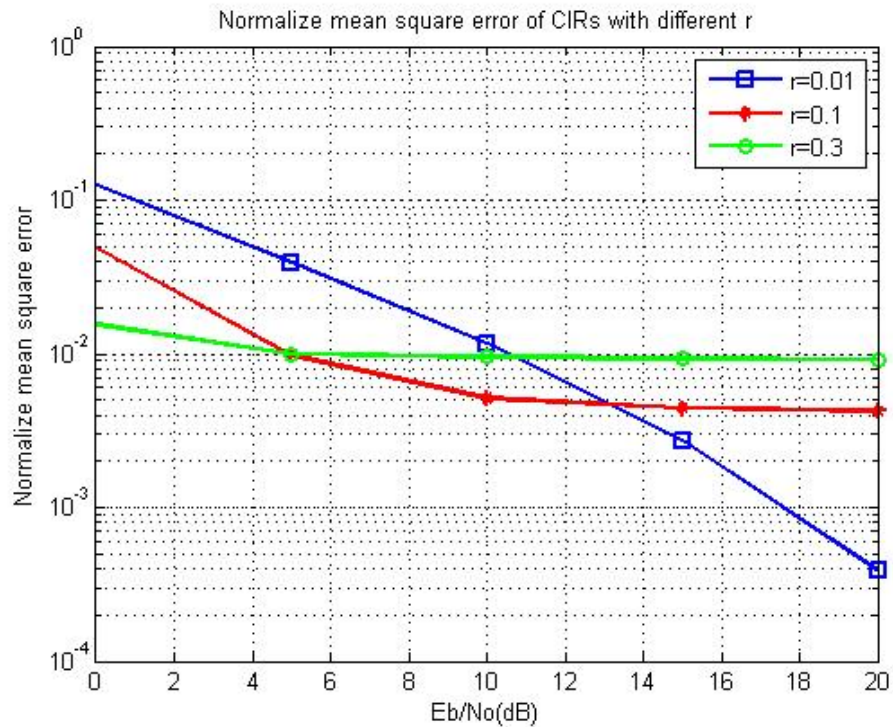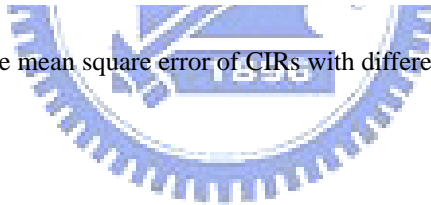


Figure 5.5 Normalize mean square error of CIRs with different γ in 2-path channel
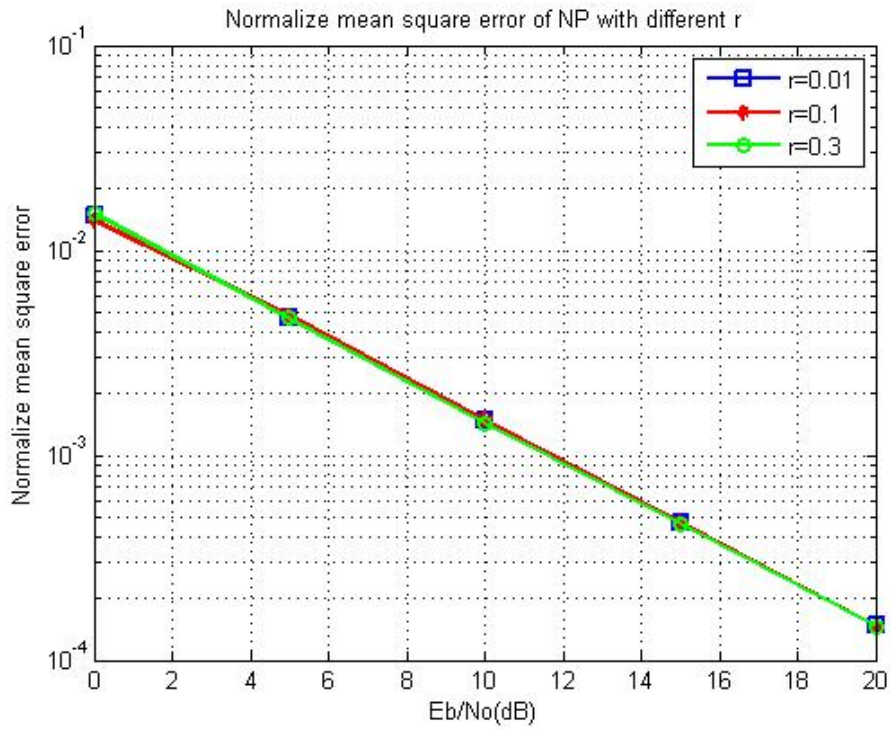
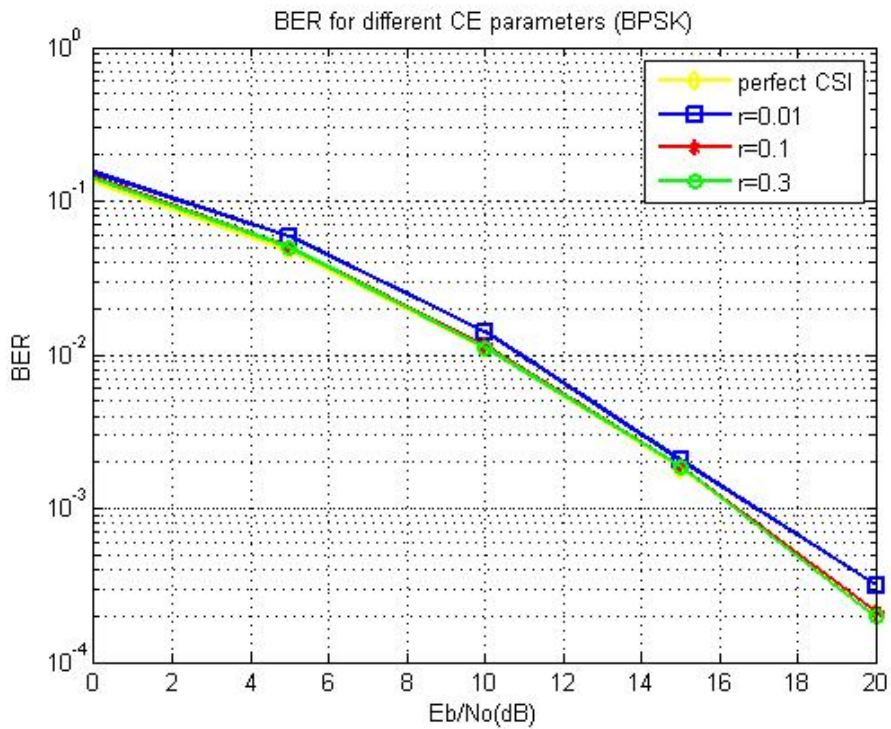Figure 5.6 Normalize mean square error of NP with different γ in 2-path channel



Figure 5.7 Performance of estimated CSI with different γ in BER for 2-path channel (BPSK)
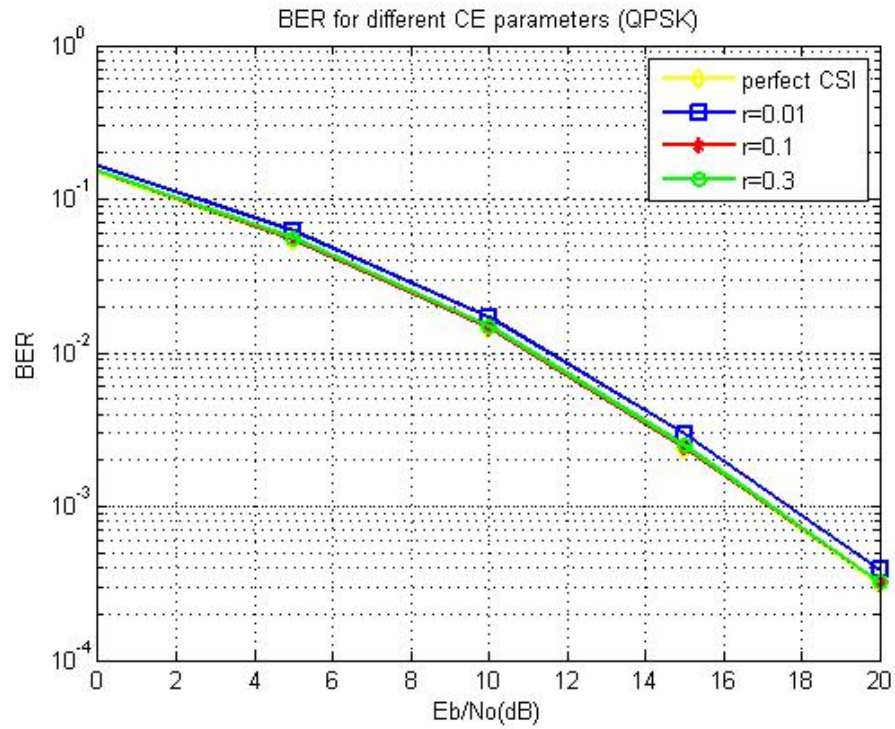
Figure 5.8 Performance of estimated CSI with different γ in BER for 2-path channel (QPSK)
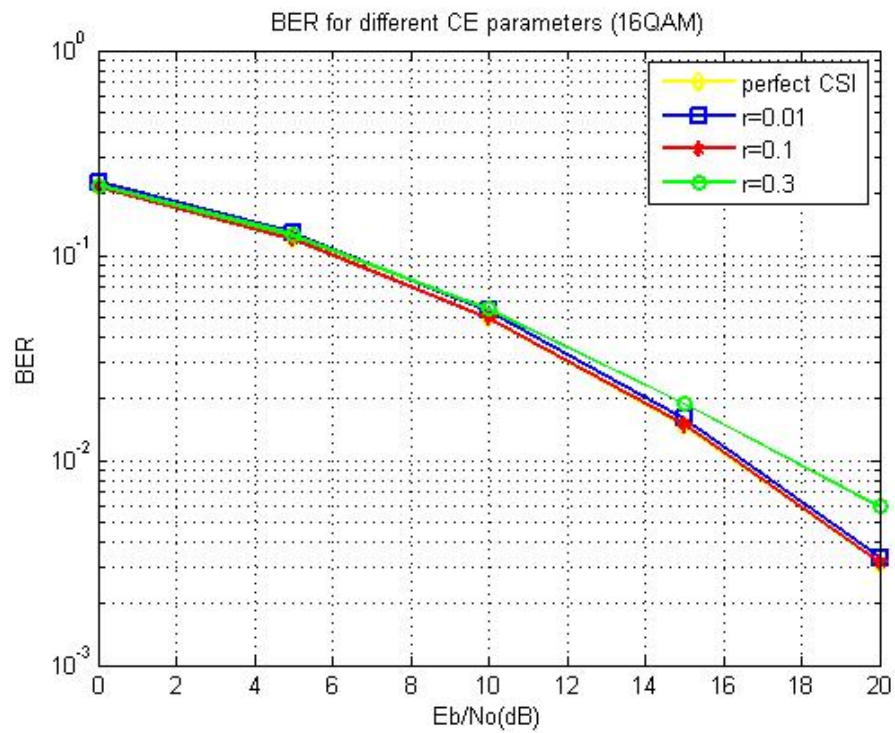


Figure 5.9 Performance of estimated CSI with different γ in BER for 2-path channel (16QAM)
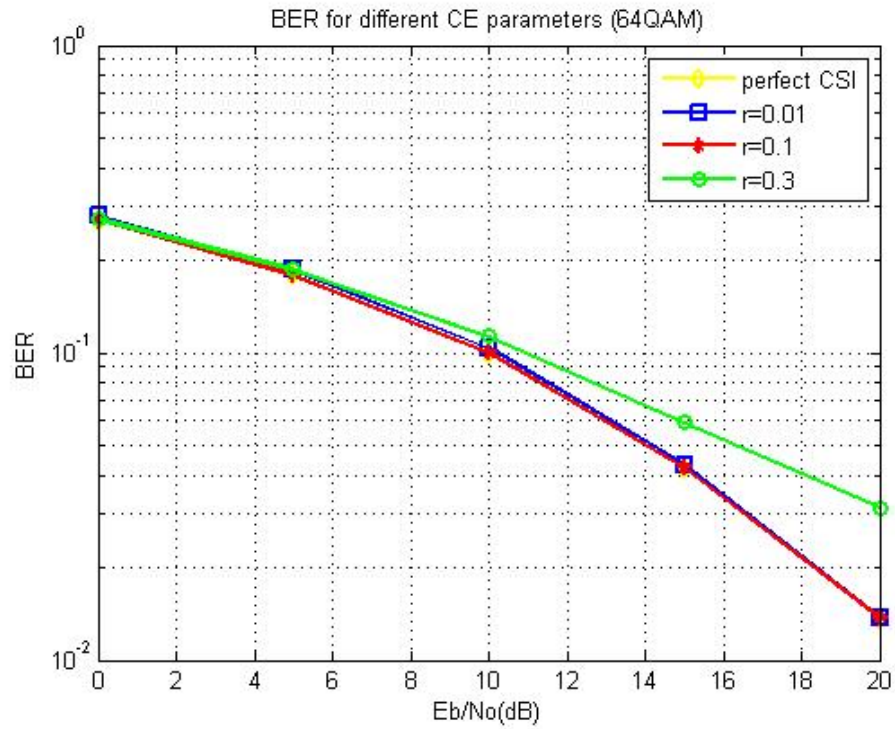
Figure 5.10 Performance of estimated CSI with different γ in BER for 2-path channel (64QAM)
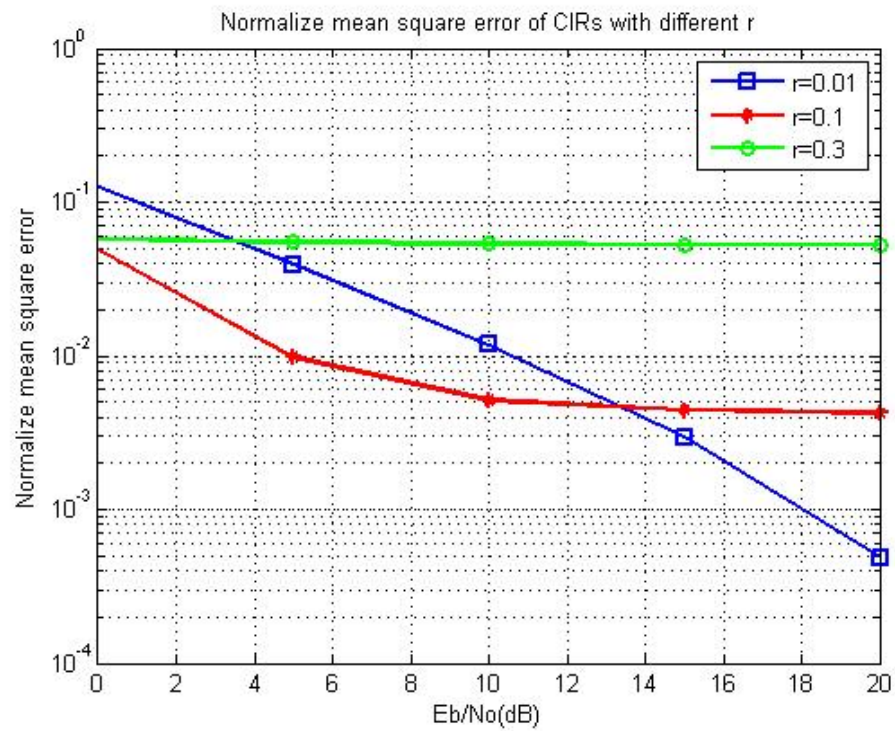


Figure 5.11 Normalize mean square error of CIRs with different γ in 6-path channel
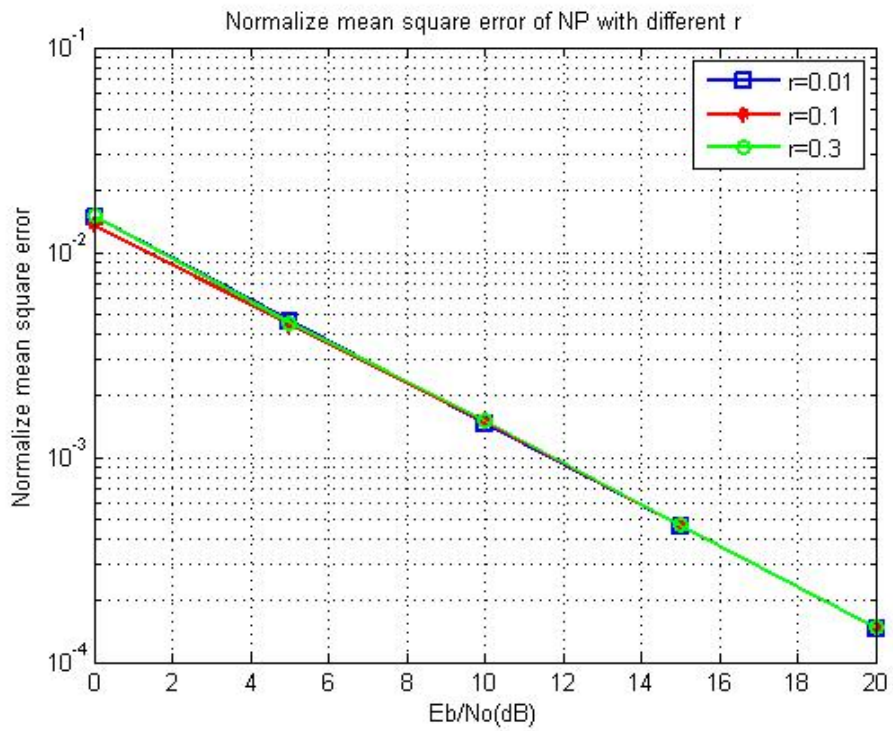
Figure 5.12 Normalize mean square error of NP with different γ in 6-path channel
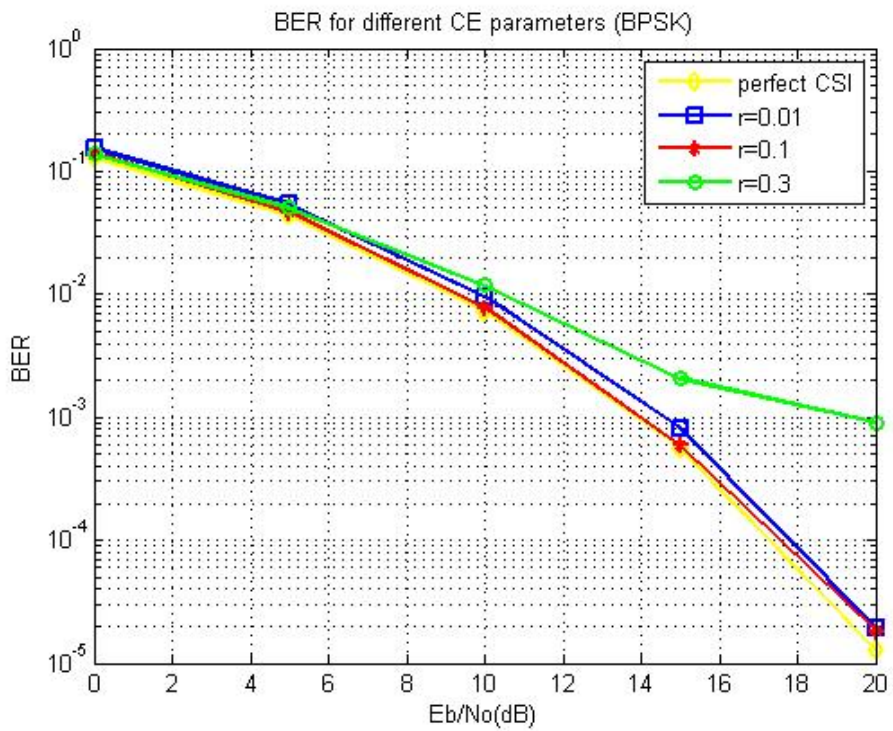


Figure 5.13 Performance of estimated CSI with different γ in BER for 6-path channel (BPSK)
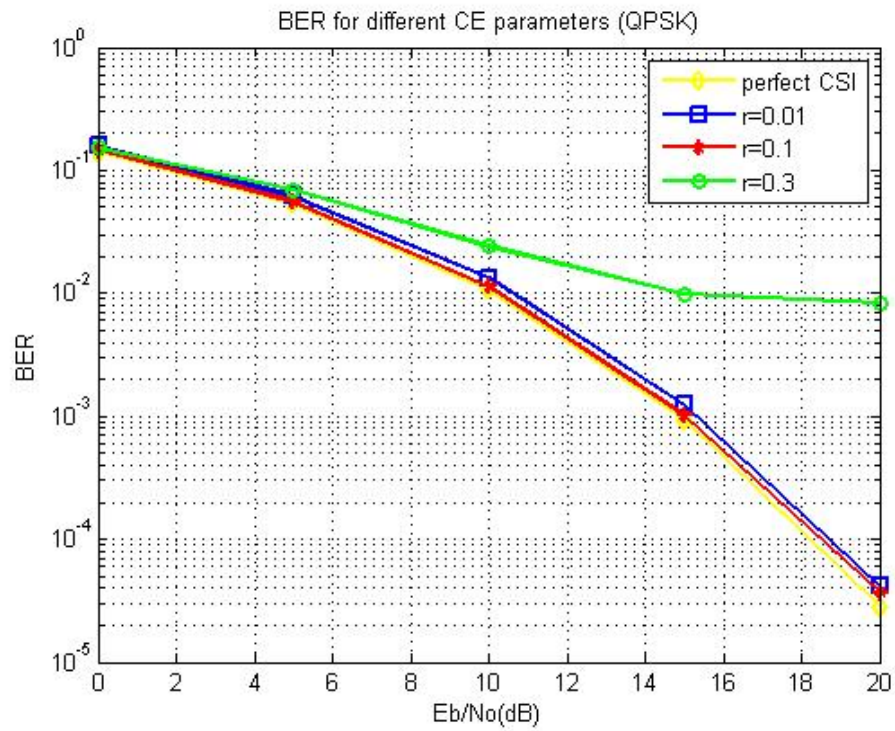
Figure 5.14 Performance of estimated CSI with different γ in BER for 6-path channel (QPSK)
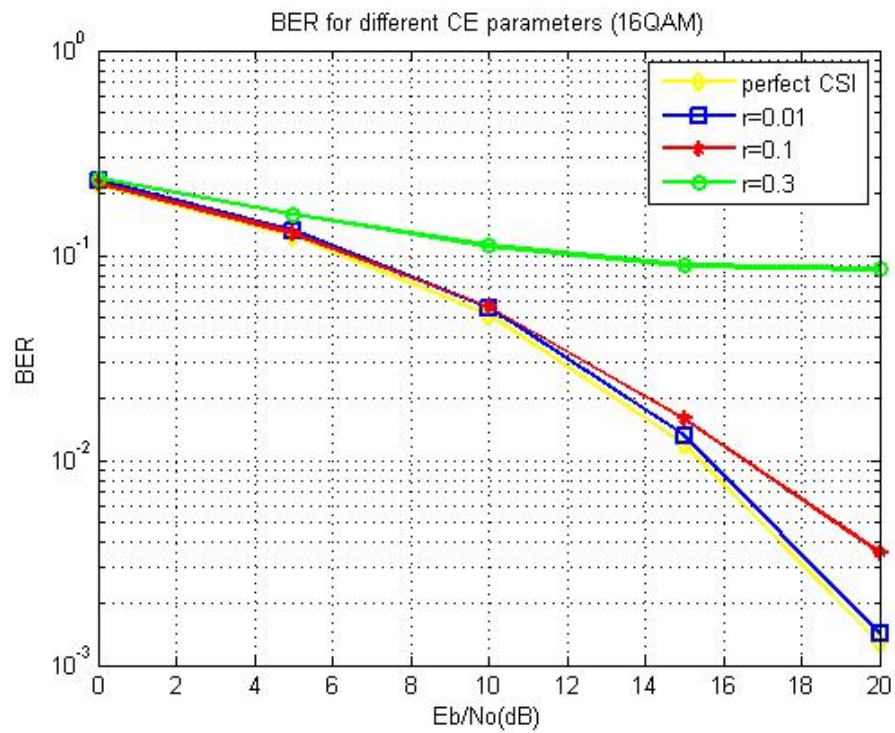


Figure 5.15 Performance of estimated CSI with different γ in BER for 6-path channel (16QAM)
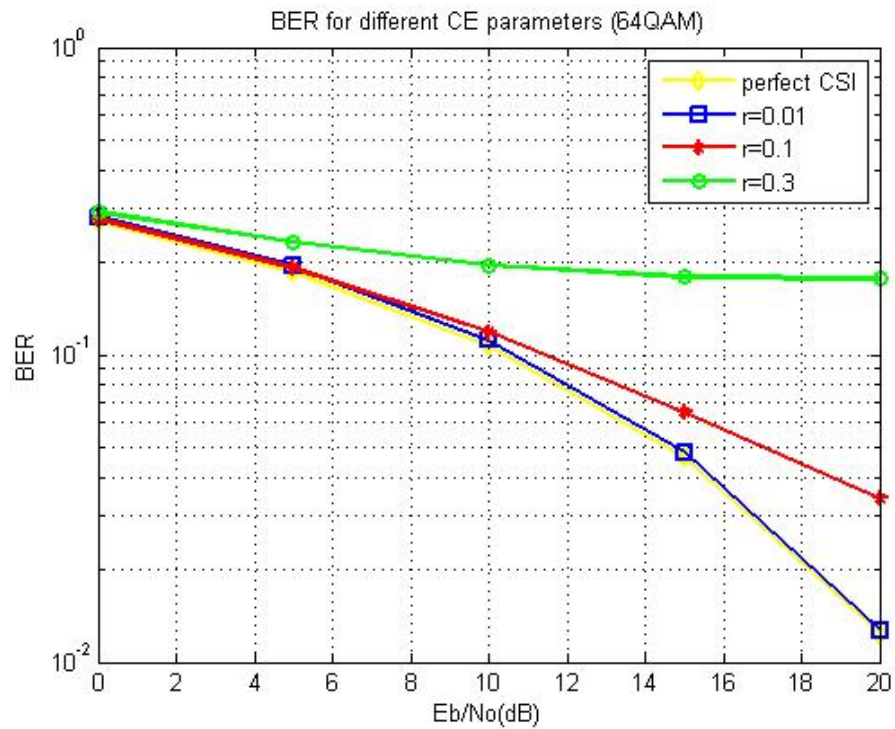
Figure 5.16 Performance of estimated CSI with different γ in BER for 6-path channel (64QAM)
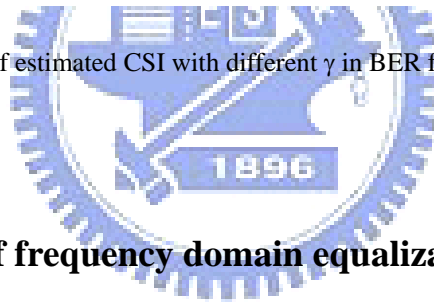
## 5.3 Simulation results of frequency domain equalization

In this section, the performances in BER for different type modulations, BPSK, QPSK,

16QAM, and 64QAM, are demonstrated in figure 5.17 and 5.18 for 2-path and 6-path channel

models respectively. The simulation parameters in this section are the same to the previous

section and listed in the table 5.5 as well. We find the performances in 6-path channel is much

better than the same modulation in 2-path channel, because that 6-path channel provides more

diversity in time domain than 2-path channel.

Figure 5.17 BER for FDE with different modulations in 2-path channel



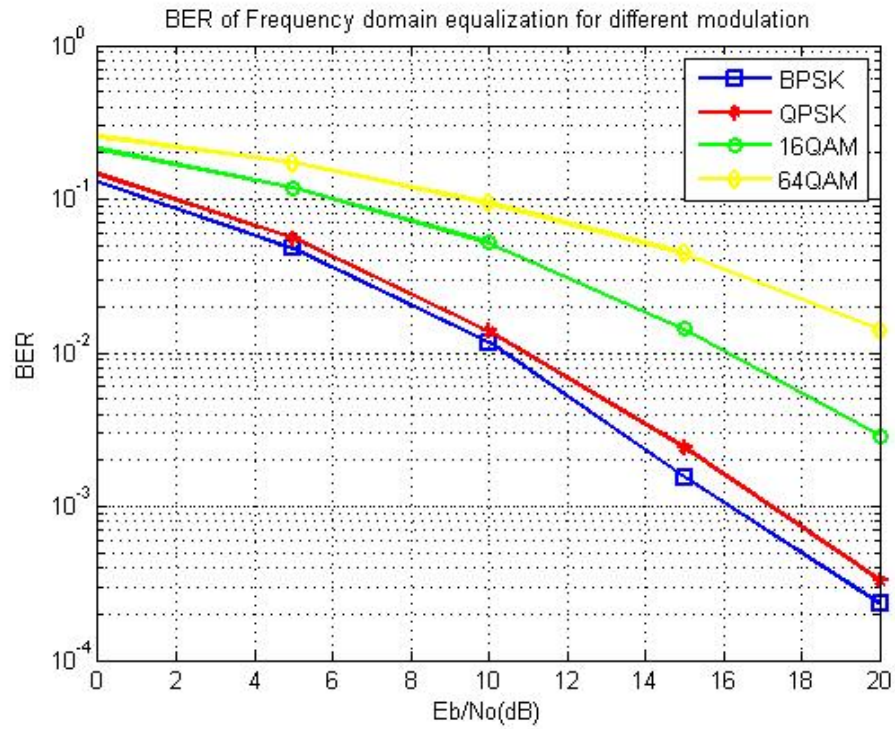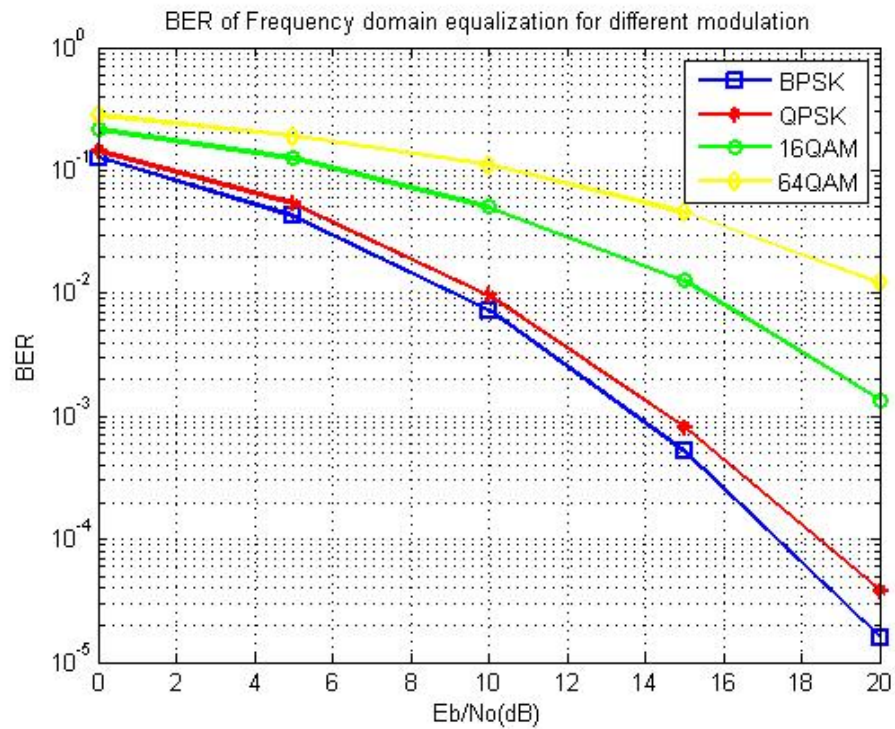Figure 5.18 BER for FDE with different modulations in 6-path channel

## 5.4 Simulation results of data detection

We compare two data detection methods, Gibbs sampler (GS) and multipath interference cancellation (MPIC) detector from figure 5.19 to figure 26 for 2-path channel model with different modulations. From these results, we know the improvements of GS and MPIC detectors are not too obvious in this case. And the different iteration numbers do not make too much difference in performance. GS detector even gets worse performances than the FDE when high order modulations at low SNR region as illustrate in figure 5.23 and 5.25. According to this situation, we say that the MPIC detector outperforms the GS detector in 2-path fading channel.



Figure 5.19 GS detector with different iteration numbers in 2-path channel (BPSK)

Figure 5.20 MPIC detector with different iteration numbers in 2-path channel (BPSK)



Figure 5.21 GS detector with different iteration numbers in 2-path channel (QPSK)

Figure 5.22 MPIC detector with different iteration numbers in 2-path channel (QPSK)



Figure 5.23 GS detector with different iteration numbers in 2-path channel (16QAM)

Figure 5.24 MPIC detector with different iteration numbers in 2-path channel (16QAM)
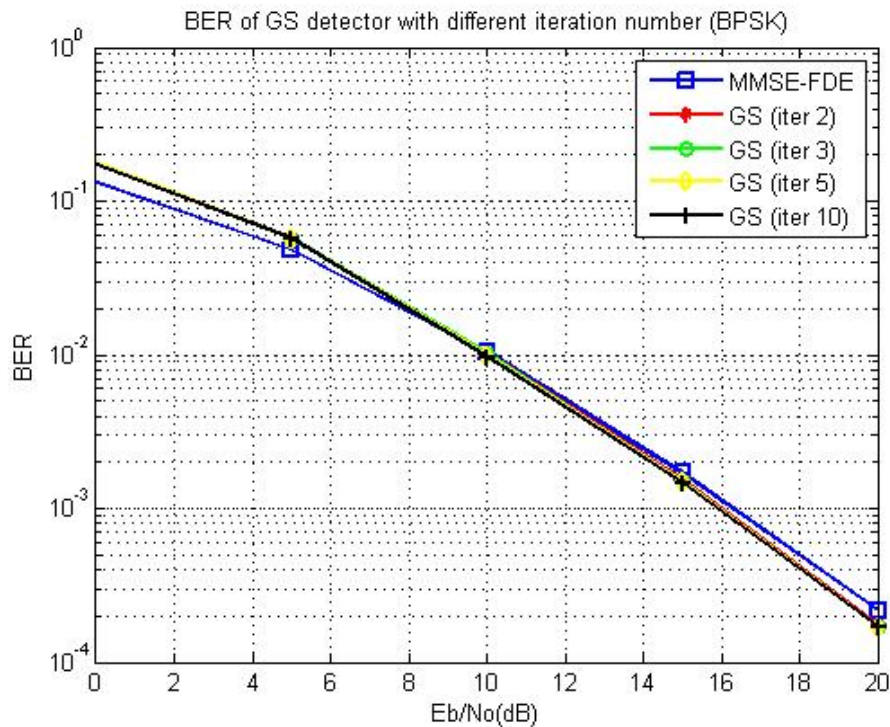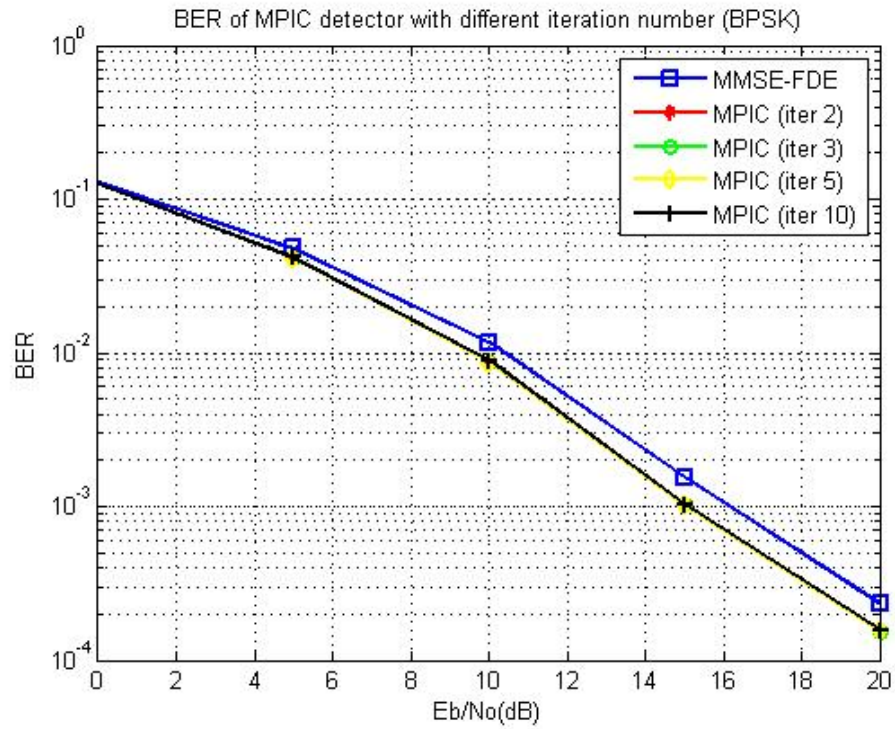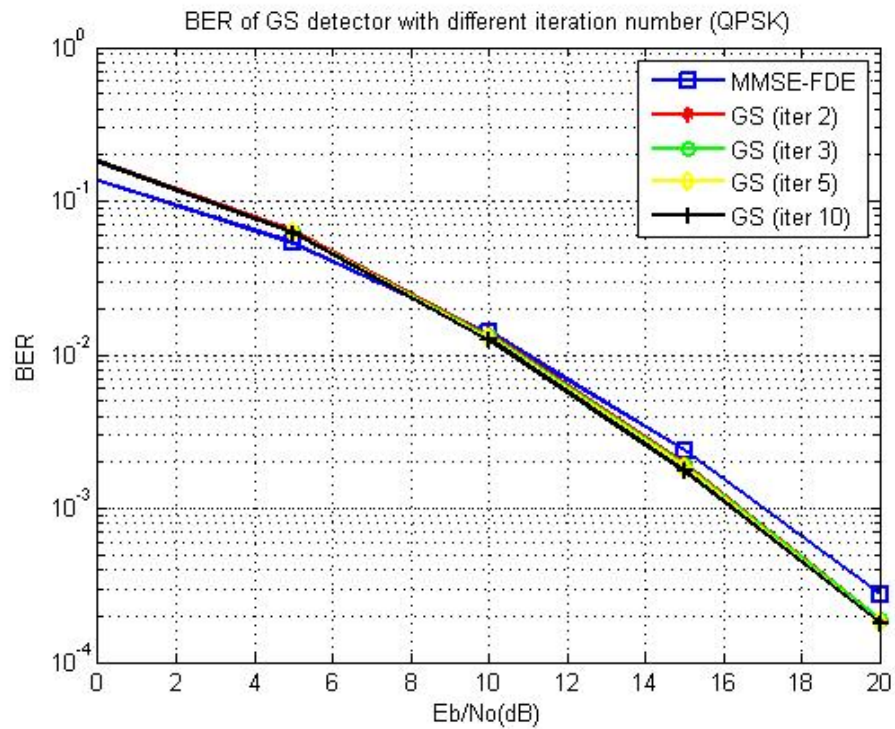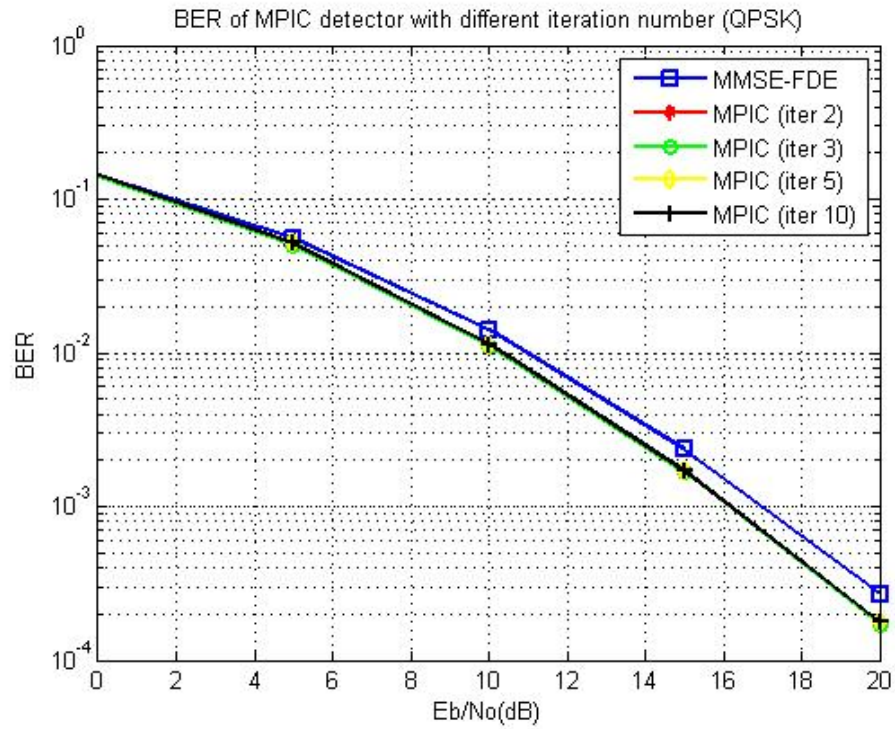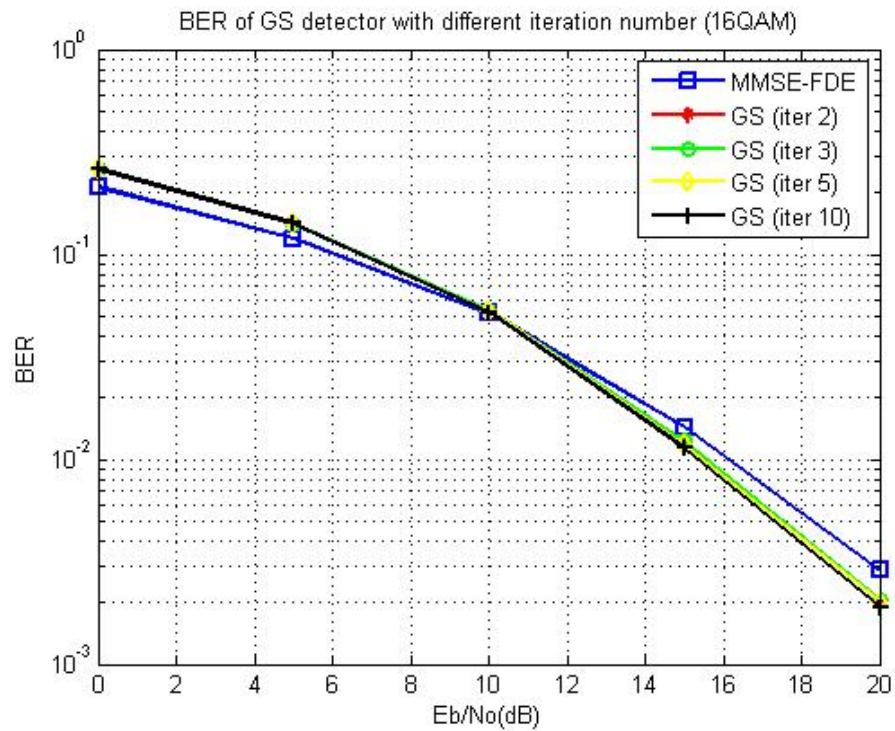


Figure 5.25 GS detector with different iteration numbers in 2-path channel (64QAM)

Figure 5.26 MPIC detector with different iteration numbers in 2-path channel (64QAM)

Now, we consider the condition in 6-path channel model. Similar to the simulations in 2-path channel, figure 5.27 to figure 34 present the performances in BER for kinds of modulations. From the results, we know that GS and MPIC detectors make the great improvements from the FDE in BPSK and QPSK modulations. For QAM modulations such as 16QAM and 64 QAM, the MPIC detector performs poor after iterations. That is because sometimes the initial values which provided by the FDE is not good enough to let the performance converges. According to our observation, MPIC detector works well when the error number of FDE is relatively small. When the initial value is not good enough, the interference term in equation 4.29 will be large. To face this situation, the performance of MPIC detector will diverge and get worse and worse after iterations. It is the reason that the

BER curve in 2 iterations outperforms the curves with more iteration numbers. More details

for this problem are shown in table 5.6. In order to solve this error propagation problem, we

can calculate the distance in the equation 4.16 after the each iteration. Then select the one

with minimum distance as our solution. By doing this operation, the computation complexity

increases lightly, but the performance in BER becomes much better than before. In

comparison between two detectors, GS does not face to this condition, the performance surely

converge after iterations. We say that the GS detector is more suitable for the situation for

high order modulations in SCBT system.
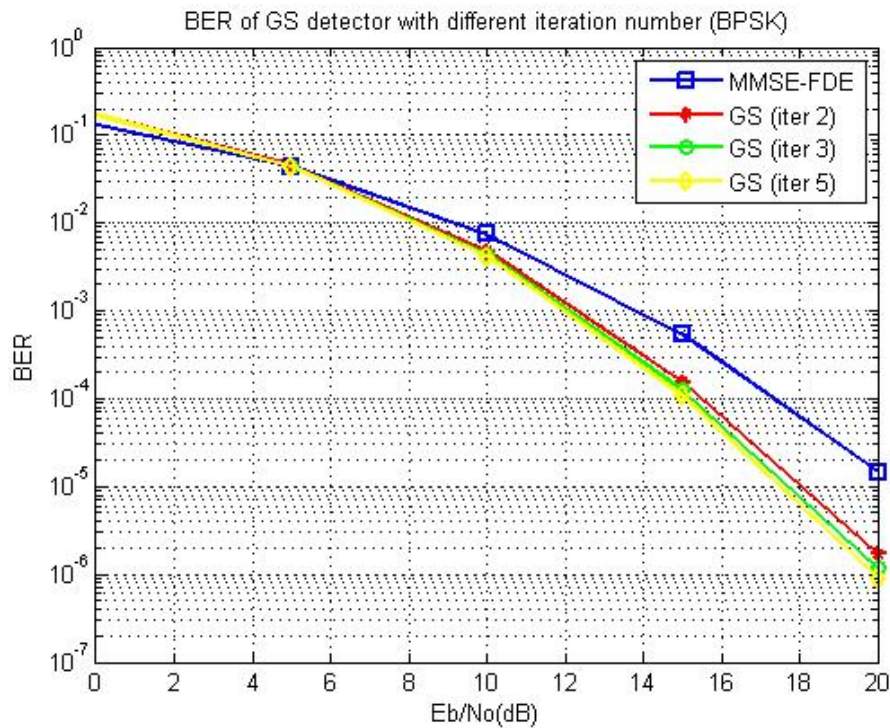


Figure 5.27 GS detector with different iteration numbers in 6-path channel (BPSK)
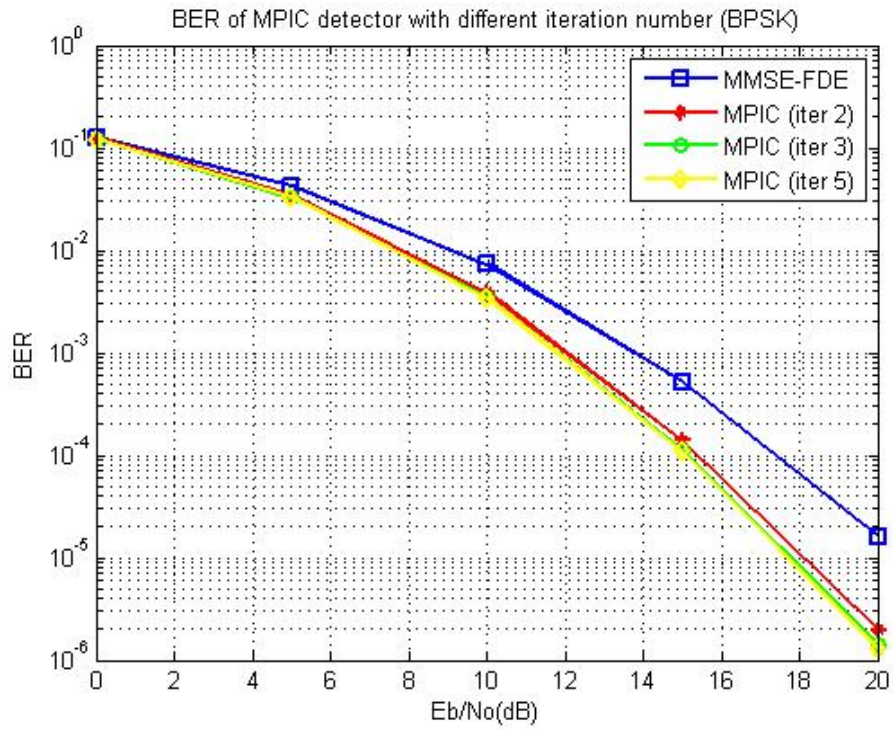
Figure 5.28 MPIC detector with different iteration numbers in 6-path channel (BPSK)
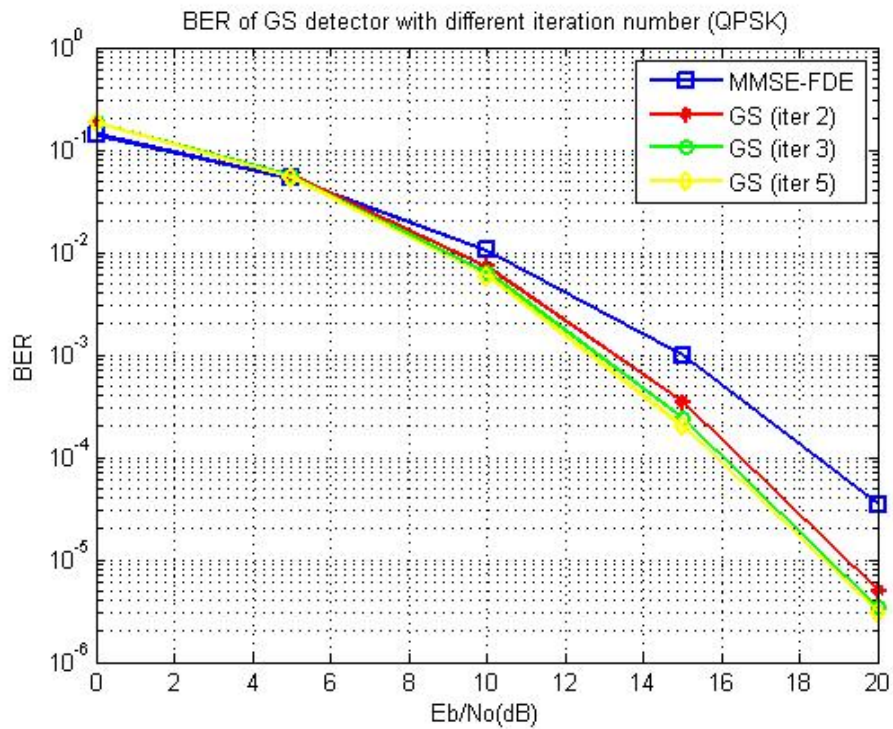


Figure 5.29 GS detector with different iteration numbers in 6-path channel (QPSK)
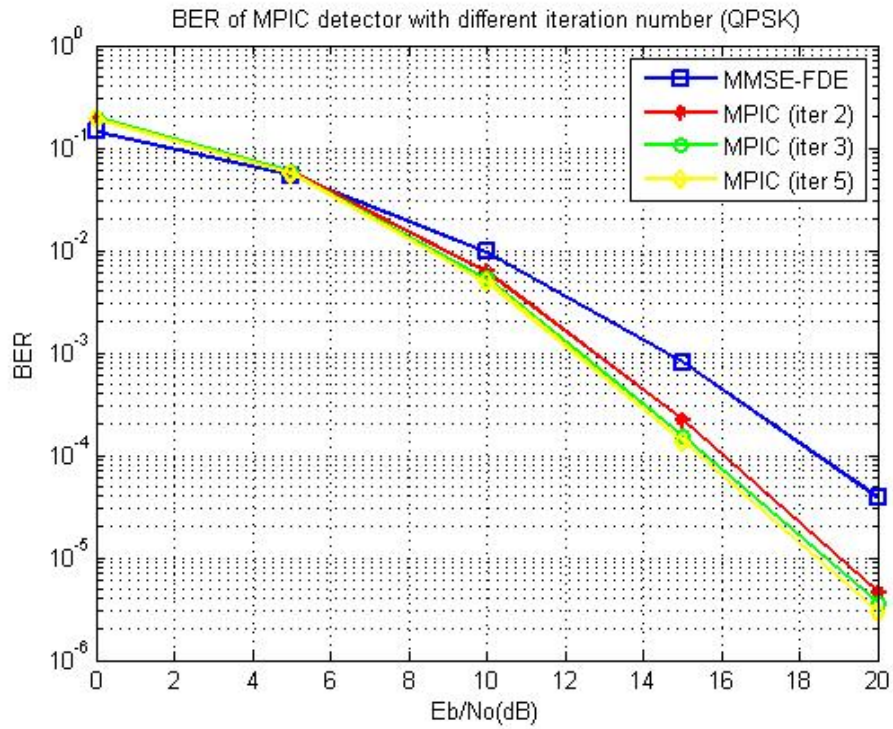
Figure 5.30 MPIC detector with different iteration numbers in 6-path channel (QPSK)
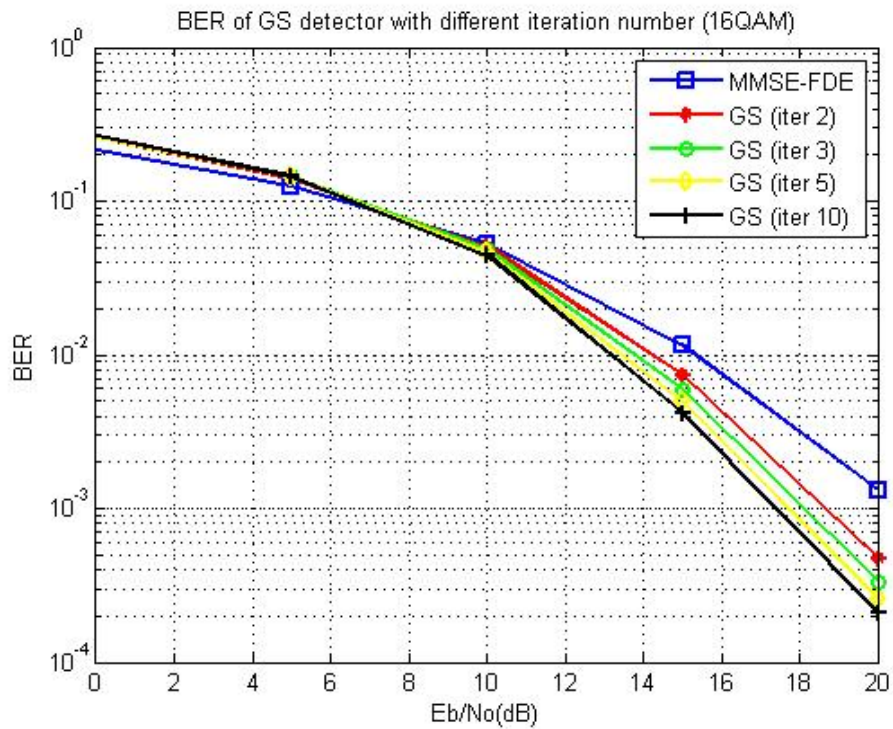


Figure 5.31 GS detector with different iteration numbers in 6-path channel (16QAM)
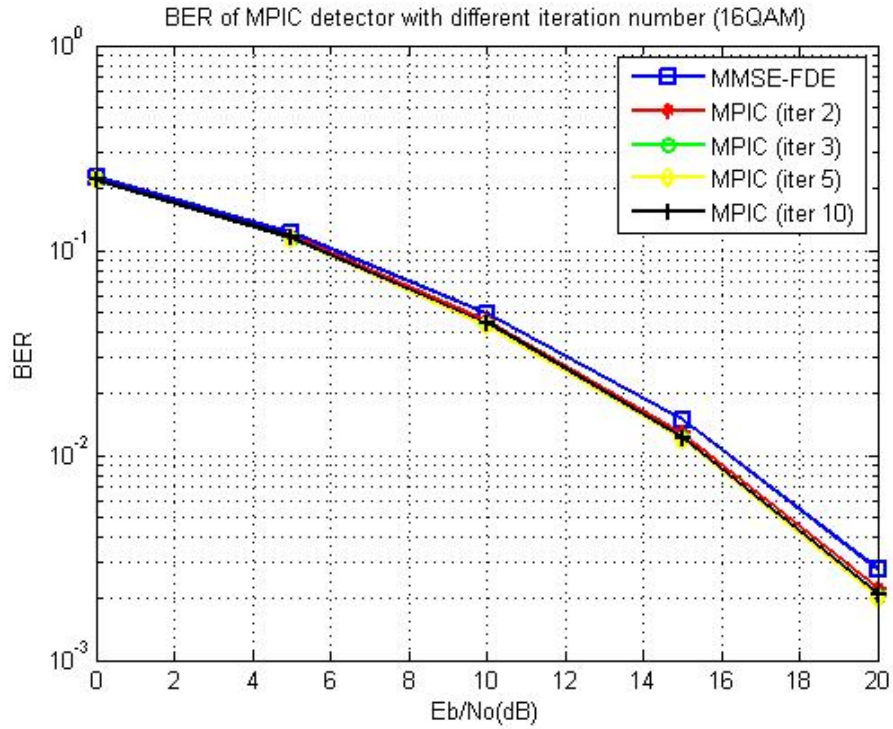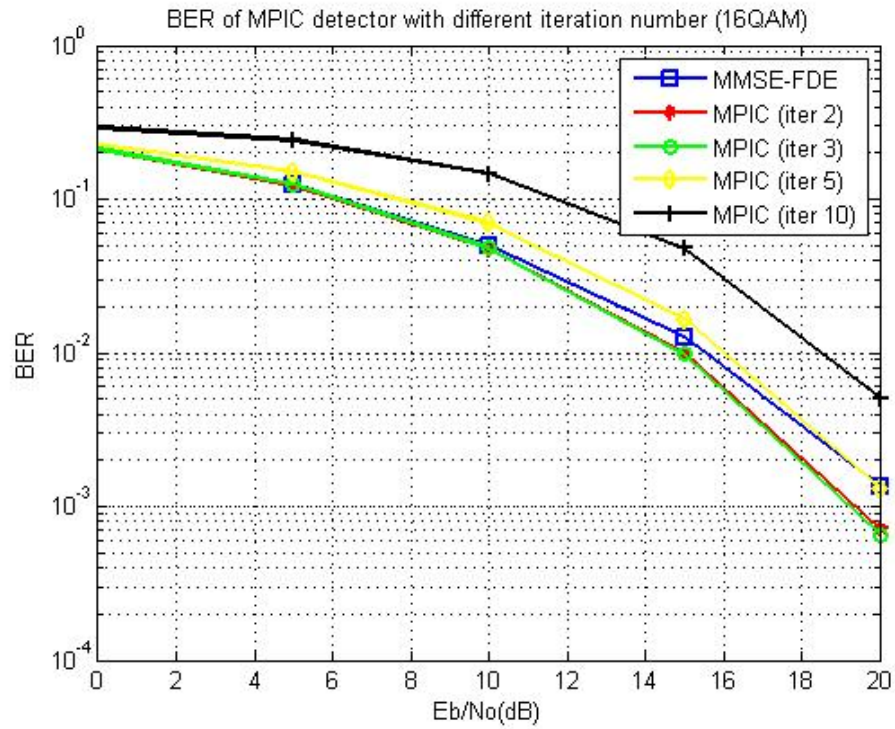
Figure 5.32 MPIC detector with different iteration numbers in 6-path channel (16QAM)
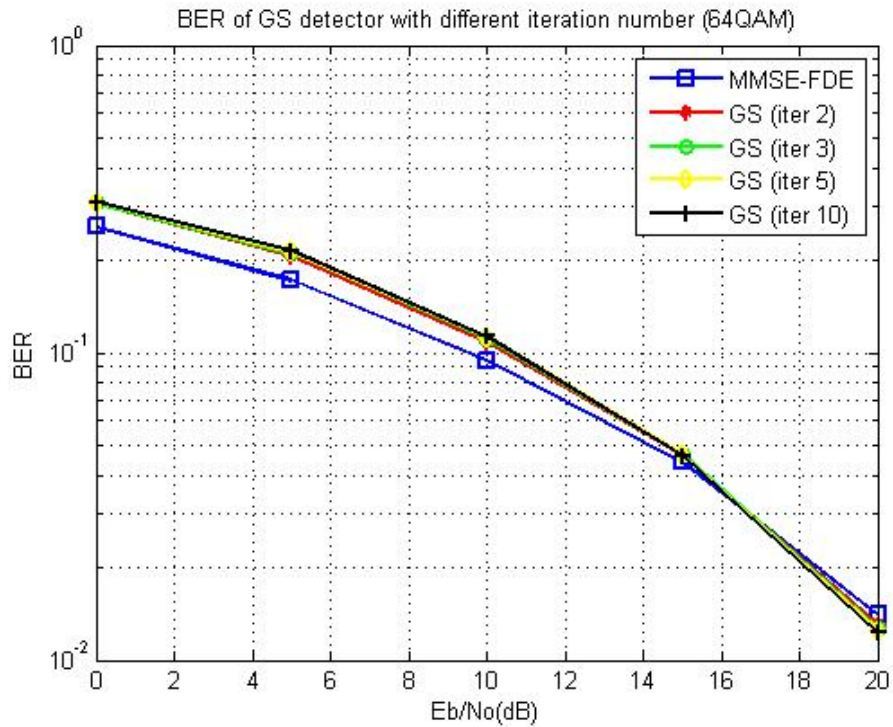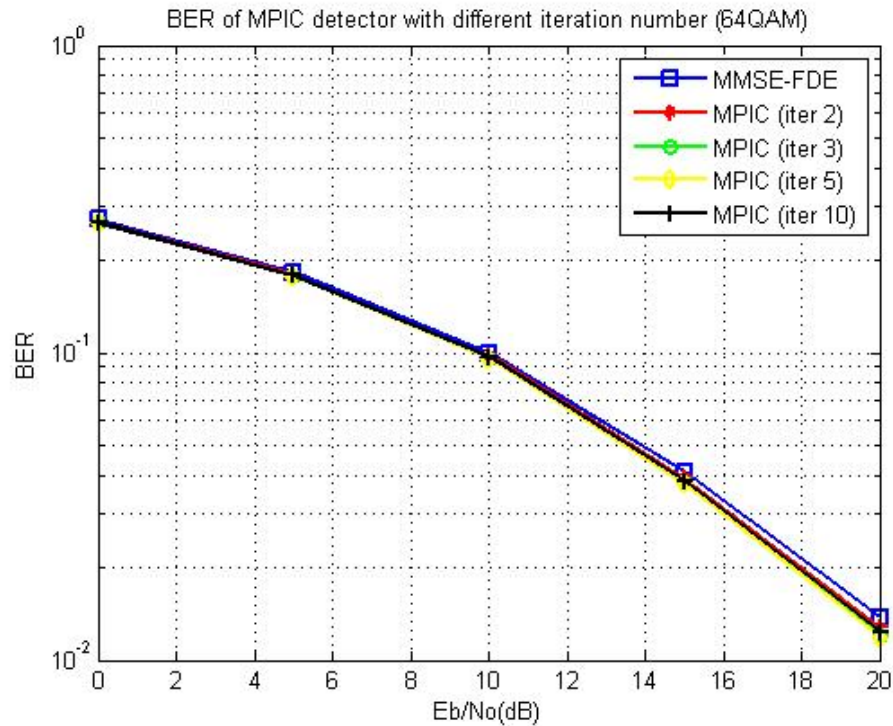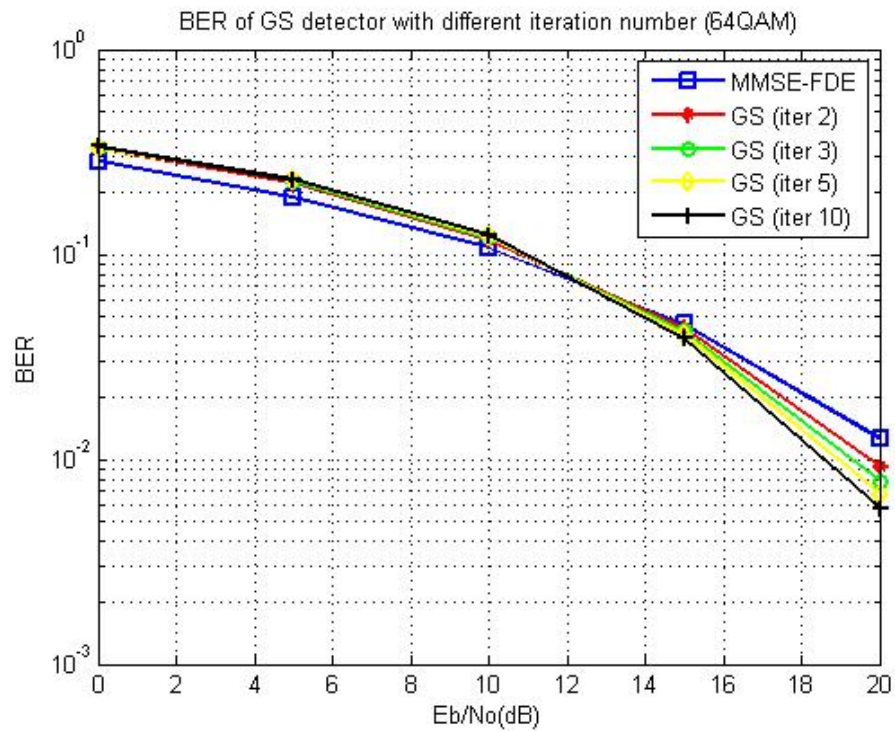


Figure 5.33 GS detector with different iteration numbers in 6-path channel (64QAM)
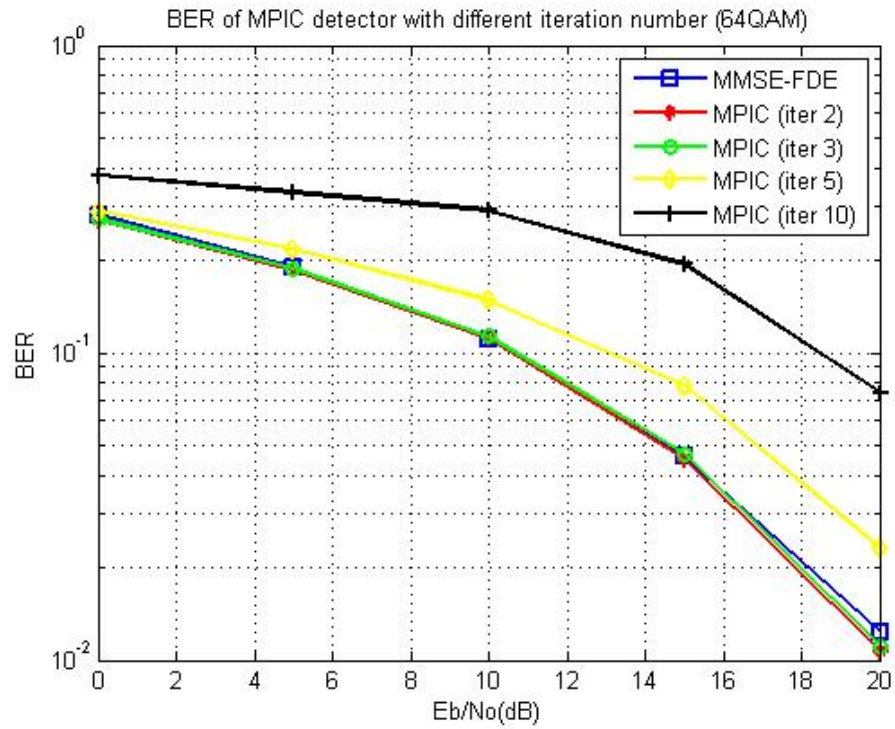
Figure 5.34 MPIC detector with different iteration numbers in 6-path channel (64QAM)

| examples | 1 | 2 | 3 | 4 | 5 | 6 | total |
|----------|---|---|---|---|---|---|-------|
| initial | 12 | 17 | 30 | 32 | 73 | 20 | 184 |
| iter 2 | 6 | 7 | 30 | 23 | 80 | 17 | 156 |
| iter 3 | 2 | 4 | 39 | 19 | 85 | 12 | 161 |
| iter 5 | 1 | 1 | 78 | 14 | 220 | 11 | 325 |
| iter 10 | 0 | 0 | 538 | 12 | 705 | 11 | 1266 |

Table 5.6 Patterns of error number after each iteration in figure 5.34

Figure 5.34 and 5.35 show the performances for different data detection methods in

BPSK transmission for 2-path and 6-path respectively. We add the BER curve of PDA

algorithm as the reference into the figure. We find that the performances of the detectors, GS and MPIC detector, that we proposed are very close to the PDA algorithm with much lower computation complexity than PDA algorithm.

Table 5.7 displays the computation complexity of each data detection method in figure 5.34 and 5.35, where $N$ is the block length of data symbols, $M$ is total number of possible symbol, $P$ is the number of paths, and $Ns$ is the iterative number of detector. For example, when the system uses BPSK transmission and the block length equals 256 in 6-path fading channel with 2 iterations for each detector, the total numbers of multiplication are also shown in the table 5.7. We can easily find the methods we proposed (GS and MPIC) can achieve the performances which are very close to PDA algorithm with much lower computation complexities.

| Methods | Multiplications | Multiplications ($N=256,M=2,P=6,Ns=2$) |
|---------|-----------------|------------------------------------------|
| MMSE-FDE | $3 \times 2N \log_2^N$ | 6144 |
| FDE+GS | $3 \times 2N \log_2^N + 2P \times M \times N \times Ns$ | 6144+12288 |
| FDE+MPIC | $3 \times 2N \log_2^N + 2P \times N \times Ns$ | 6144+6144 |
| PDA | $N(N^2 + 2P(N+2) + N)Ns$ | 35270656 |

Table 5.7 Complexity of each data detection method
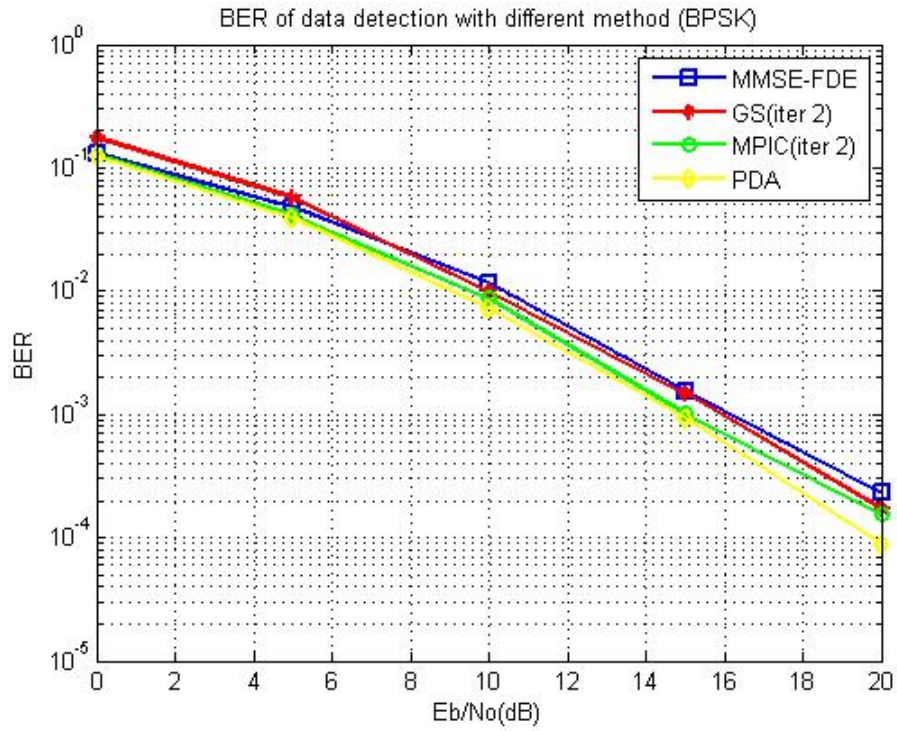
Figure 5.35 Different data detection methods in 2-path channel (BPSK)
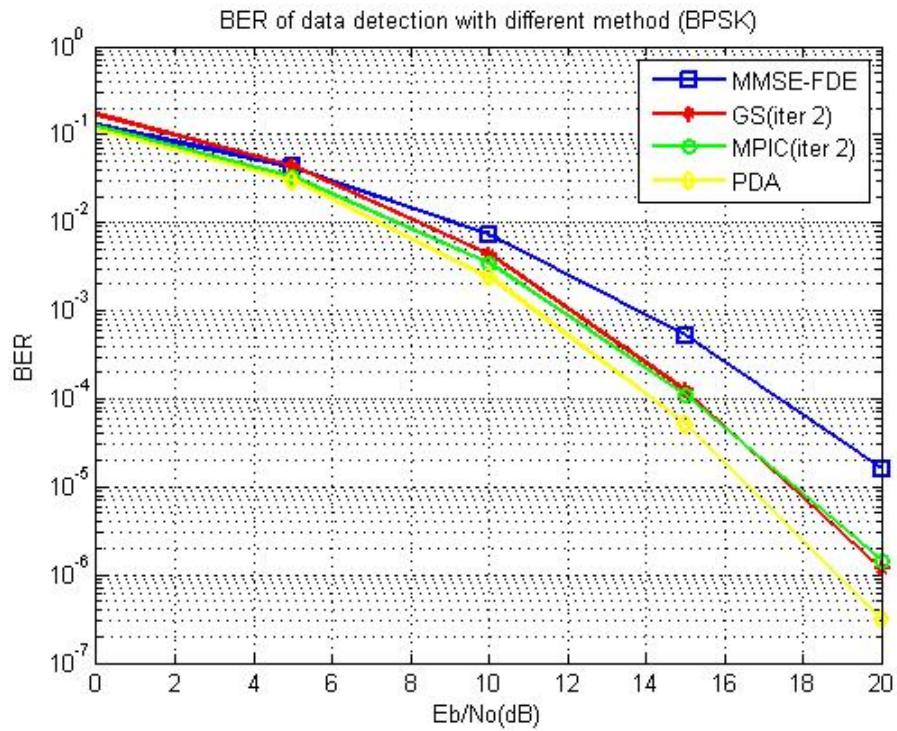


Figure 5.36 Different data detection methods in 6-path channel (BPSK)

## Chapter 6 Conclusions

In this thesis, we design a baseband receiver for IEEE 802.15.3c SCBT system with relatively lower computation complexity than other systems. And we do the computer simulations to verify the performances of the methods that we proposed. In synchronization part, the method that we used can improve the probability of tracking on the timing of first path. And the overall probability of error (symbol timing is outside the ISI free region) is very low. Because the symbol in the synchronization sequence is either +1 or -1, then the multiplications in the algorithm can be replaced by adders and inverters to reduce the complexity of implementation. For channel estimation, we use the auto-correlation property of Golay complementary sequences to design our CE algorithm for CIRs and noise power. The performance illustrates that the estimated CSI performs almost the same as the perfect CSI when the threshold is chosen correctly. As the same reason in synchronization, the circuit design in channel estimation part is also very simple. At last, the data detection methods we proposed improve the BER performance after FDE. We also do the simulations for different type modulations such as PSK and QAM modulations. User can choose the proper modulations according to the requirements of throughput (data rate) and BER by referring our simulation results.

In this paper, we assume the CIRs are fixed during a packet slot. In future work, we may consider the time varying channel during a data block and modify the CE algorithm on

tracking the variation of the channel. According to the IEEE 802.15.3c standard, the Reed

Solomon and LDPC codes can be use in channel coding to enhance the system performance.

The analysis of SCBT with channel coding is another potential research issue and direction. In

IEEE 802.15.3c standard, the OFDM system is coexistent with SCBT system, so the

transceiver design of OFDM is also a research direction. Moreover, how to implement the

dual-mode system let the OFDM and the SCBT systems can operate simultaneously becomes

another important issue in the future.

## Appendix A. Complexity of Gibbs sampler algorithm in SCBT system

In GS algorithm, we need to calculate the probability $p(x_n \mid \boldsymbol{y}, x_1, \cdots, x_{n-1}, x_{n+1}, \cdots, x_N)$. To simplify the equation, we define

$$\boldsymbol{x}_{-n} = [x_1, \cdots, x_{n-1}, x_{n+1}, \cdots, x_N]^{\mathrm{T}}. \tag{A.1}$$

where T is the vector transpose.

Assume that $x_n \in [m_1 \ m_2 \cdots m_M]$ where $M$ is the number of possible symbols for $x_n$. Then the equation 4.30 can be rewritten as

$$p(x_n = m_j \mid \boldsymbol{y}, \boldsymbol{x}_{-n}) = \frac{p(\boldsymbol{y} \mid \boldsymbol{x})_{x_n = m_j}}{\sum_{m=1}^{M} p(\boldsymbol{y} \mid \boldsymbol{x})_{x_n = m_m}}. \tag{A.2}$$

After we derive the equation 4.30 and define the distance vector $\boldsymbol{d}_i = \boldsymbol{y} - H\boldsymbol{x}_{x_n = m_i}$, we have following relationship

$$p(x_n = m_j \mid \boldsymbol{y}, \boldsymbol{x}_{-n}) \propto \exp\left(-\frac{\|\boldsymbol{y} - H\boldsymbol{x}\|^2_{x_n = m_j}}{2\sigma^2}\right) = \exp\left(-\frac{\|\boldsymbol{d}_j\|^2}{2\sigma^2}\right) \tag{A.3}$$

We also know that

$$H\boldsymbol{x} = \begin{bmatrix} \boldsymbol{h}_1 & \boldsymbol{h}_2 & \cdots & \boldsymbol{h}_N \end{bmatrix} \begin{bmatrix} x_1 \\ x_2 \\ \vdots \\ x_N \end{bmatrix} = \sum_{k=1}^{N} \boldsymbol{h}_k x_k \tag{A.4}$$

where $\boldsymbol{h}_n$ is the vector $[\boldsymbol{h} \ \boldsymbol{0}]^T$ circular shift $n$-1 elements.

The distance vector $\boldsymbol{d}_j$ can be expressed as

$$\boldsymbol{d}_j = \boldsymbol{y} - H\boldsymbol{x}_{x_n = m_j} = \boldsymbol{y} - \boldsymbol{h}_n m_j - \sum_{k=1, k \neq n}^{N} \boldsymbol{h}_k x_k. \tag{A.5}$$

Now we focus on the relationship between $\boldsymbol{d}_j$ and $\boldsymbol{d}_i$

$$d_i = y - Hx_{x_n=m_i} = y - (Hx_{x_n=m_j} - h_n m_j + h_n m_i) = d_j + \underbrace{h_n(m_j - m_i)}_{P \text{ multiplications}}. \qquad \text{(A.6)}$$

From above equation, we know that there are $P$ multiplications to calculate $d_j$ form $d_i$

where $P$ is the number of paths. Now we modify the equation A.2 as follow

$$p(x_n = m_i \mid y, x_{-n}) = \frac{p(x_n = m_i \mid y, x_{-n})}{\sum_{m=1}^{M} p(x_n = m_m \mid y, x_{-n})} = \frac{\exp(-\frac{\|d_i\|^2}{2\sigma^2})\exp(\frac{\|d_j\|^2}{2\sigma^2})}{(\sum_{m=1}^{M}\exp(-\frac{\|d_m\|^2}{2\sigma^2}))\exp(\frac{\|d_j\|^2}{2\sigma^2})}$$

$$= \frac{\exp(-\frac{\|d_i\|^2 - \|d_j\|^2}{2\sigma^2})}{\sum_{m=1}^{M}\exp(-\frac{\|d_m\|^2 - \|d_j\|^2}{2\sigma^2})}. \qquad \text{(A.7)}$$

According to our observation, we find that only $P$ elements in the vector $d_j$ and $d_i$ are

different. By using this property, the equation $\|d_i\|^2 - \|d_j\|^2$ can be simplified as

$$\|d_i\|^2 - \|d_j\|^2 = \|d_i^{'}\|^2 - \|d_j^{'}\|^2, \qquad \text{(A.8)}$$

and

$$\|d_i^{'}\|^2 - \|d_j^{'}\|^2 = \sum_{p=1}^{P}(|d_i[k]|^2 - |d_j[k]|^2)$$

$$= (\sum_{p=1}^{P}(\|y[((n+\tau_p-2))_N+1] - Hx_{x_n=m_j}[((n+\tau_p-2))_N+1] + h_p(m_j - m_i)\|^2)$$

$$-\sum_{p=1}^{P}(\|y[((n+\tau_p-2))_N+1] - Hx_{x_n=m_j}[((n+\tau_p-2))_N+1]\|^2)) \qquad \text{(A.9)}$$

where $d_i^{'}$ is the vector of elements in $d_i$ which are different to $d_j$. From above derivation,

we need other $P$ multiplications to calculate $\|d_i\|^{2'} = \|d_i\|^2 - \|d_{x_n^{(n_s-1)}}\|^2$ in Gibbs algorithm. To

summarize, $2P \times M \times N$ multiplications per iteration and $2P \times M$ multiplications per

symbol are needed, where $N$ is the length of data symbols. If the Gibbs sampler iterates $Ns$

times, there are $2P \times M \times N \times Ns$ multiplications in total for this process.

# References

[1] **"IEEE 802.15-07-0934-01-003c"**, http://www.ieee802.org/15/pub/TG3c.html.

[2] Zhengdao Wang, Xiaoli Ma, and G. B. Giannakis, **"OFDM or single-carrier block transmissions?",** IEEE Transactions on Communications, Vol. 52, Issue 3, pp. 380-394, March 2004.

[3] R. Funada, H. Harada, and others, **"A design of single carrier based PHY for IEEE 802.15.3c standard"**, IEEE 18th International Symposium on Personal Indoor and Mobile Radio Communications, PIMRC 2007, pp. 1-5, September 2007.

[4] D. Falconer, S. L. Ariyavisitakul, A. Benyamin-Seeyar, and B. Eidson, **" Frequency domain equalization for single-carrier broadband wireless systems",** IEEE Communication Magazine, Vol. 40, Issue 4, pp. 58-66, April 2002.

[5] Jun Yang and M. Eyvazkhani, **"Adaptive Synchronization for Gbps Single-Carrier 60 GHz Wireless Systems"**, 2008 IEEE Sarnoff Symposium, pp. 1-5, April 2008.

[6] B. Xu and G. Bi, **"Channel estimation using complementary sequence pairs for UWB/OFDM systems"**, Electronics Letters, Vol. 40, Issue 19, pp. 1196- 1197, September 2004.

[7] Meng-Lin Ku and Chia-Chi Huang, **"A complementary codes pilot-based transmitter diversity technique for OFDM systems"**, IEEE Transactions on Wireless Communications, Vol. 5, Issue 3, pp. 504- 508, March 2006.

[8] M. Golay, **"Complementary series"**, IRE Transactions on Information Theory, Vol. 7, Issue 2, pp. 82-87,April 1961.

[9] N. Benvenuto and S. Tomasin, **"On the comparison between OFDM and single carrier modulation with a DFE using a frequency-domain feed-forward filter"**, IEEE Transactions on Communications, Vol. 50, Issue 6, pp. 947-955, June 2002.

[10] Ming Lei, I. Lakkis, H. Harada, and S. Kato, **"MMSE-FDE Based on Estimated SNR for Single-Carrier Block Transmission (SCBT) in Multi-Gbps WPAN (IEEE 802.15.3c)"**, 2008 ICC Workshops '08. IEEE International Conference on Communications Workshops, pp. 52 – 56, May 2008.

[11] George Casella and Edward I. George, **"Explaining the Gibbs Sampler",** The American Statistician, Vol. 46, No. 3, pp. 167-174, August 1992.

[12] Xiaodong Wang and Rong Chen, **"Adaptive Bayesian multiuser detection for synchronous CDMA with Gaussian and impulsive noise",** IEEE Transactions on Signal Processing, Vol. 48, Issue 7, pp. 2013-2028, July 2000.

[13] Xuehong Mao, P. Amini, and B. Farhang-Boroujeny, **"Markov Chain Monte Carlo MIMO Detection Methods for High Signal-to-Noise Ratio Regimes"**, IEEE Global Telecommunications Conference GLOBECOM '07. 2007, pp. 3979-3983, November 2007.

[14] J. Luo, K.R. Pattipati, P.K. Willett, and F. Hasegawa, **" Near-optimal multiuser detection in synchronous CDMA using probabilistic data association",** Communications Letters of IEEE, Vol. 5, Issue 9, pp.361-363, September 2001.

[15] Shoumin Liu and Zhi Tian, **"Near-optimum soft decision equalization for frequency selective MIMO channels"**, IEEE Transactions on Signal Processing, Vol. 52, Issue 3, pp. 721-733, March 2004.

[16] B. Hassibi and H. Vikalo, **"On the sphere-decoding algorithm I. Expected complexity",** IEEE Transactions on Signal Processing, Vol. 53, Issue 8, Part 1, pp. 2806-2818, August 2005.